

Improving the post-fire performance of reinforced concrete beams with lightweight plaster

Daniel Paul Thanaraj^a, Varun Sabu Sam^a, N. Anand^{a,*}, Diana Andrushia^b, Katherine A. Cashell^{c,*}

^a Department of Civil Engineering, Karunya Institute of Technology and Sciences, Coimbatore, India

^b Department of Electronics and communications Engineering, Karunya Institute of Technology and Sciences, Coimbatore, India

^c Department of Civil Engineering and Geomatic Engineering, UCL, GMO1 Chadwick Building, Gower St, London WC1E 6AE, United Kingdom

ARTICLE INFO

Keywords:

Reinforced Concrete
Post-fire
Fire protection
Expanded vermiculite
Expanded perlite
Testing

ABSTRACT

Structural fires pose significant risks to the built environment, making fire resistance a critical design consideration for reinforced concrete (RC) structures. Elevated temperatures during fires reduce the strength and stiffness of both concrete and steel reinforcement, compromising load-bearing capacity. This experimental study evaluates the effectiveness of lightweight plaster coatings in enhancing the post-fire performance of RC members exposed to ISO 834 standard fire conditions. Two materials, expanded vermiculite (EV) and expanded perlite (EP), were examined. First, the compressive strength of concrete mixes incorporating EV or EP as partial replacements (2.5 %, 5 %, 7.5 %, and 10 %) for fine aggregates was assessed after heating durations of 30–120 min. Subsequently, structural performance was tested in RC beams across three configurations: (1) EV or EP integrated into the mix, (2) EV or EP applied as external plaster, and (3) a combination of both. A total of 54 RC beam specimens were cast, with 12 beams used for internal temperature monitoring and 42 subjected to four-point bending tests following 60, 90, and 120 min of heating. Concrete grades M20 and M50 were developed using EV or EP as partial sand replacements, while plaster layers were prepared with EV or EP mortar. Key performance indicators, including load-deflection response, ultimate load, internal temperature distribution, residual rebar yield strength, and first-crack load, were analysed. The protected M20-EP+EPC beam recorded a 62.2 % reduction in rebar temperature compared to the unprotected M20-R beam. Further, the loss of yield strength was reduced by 87.5 %, and the moment of resistance degradation was reduced by 61.1 % compared to the unprotected M20-R beam. Beams protected with EV or EP in both the mix and external plaster demonstrated superior performance, extending survival time from 45 to 120 min and improving fire resistance ratings from 15 to 60 min based on insulation criteria.

1. Introduction

The fire performance of load-bearing structures is a critical aspect of building design, given the potentially catastrophic

* Corresponding authors.

E-mail addresses: tdanielpaul@karunya.edu (D.P. Thanaraj), varunsamsabu@gmail.com (V.S. Sam), nanand@karunya.edu (N. Anand), diana@karunya.edu (D. Andrushia), k.cashell@ucl.ac.uk (K.A. Cashell).

<https://doi.org/10.1016/j.cscm.2025.e04918>

Received 1 April 2025; Received in revised form 1 June 2025; Accepted 10 June 2025

Available online 14 June 2025

2214-5095/© 2025 The Author(s). Published by Elsevier Ltd. This is an open access article under the CC BY license (<http://creativecommons.org/licenses/by/4.0/>).

consequences of fire, including structural collapse and loss of life [3,28,31]. Although severe fire events are relatively infrequent, exposure to high temperatures can significantly degrade material properties, compromise structural integrity, and reduce load-carrying capacity, thereby endangering safe evacuation and occupant survival [45,46,53]. These risks have driven extensive research into the development of fire-resistant materials.

Among emerging solutions, expanded vermiculite (EV) and expanded perlite (EP) have gained attention for their thermal insulation capabilities. These lightweight, non-structural mineral aggregates possess low density and excellent fire resistance characteristics, making them promising candidates for enhancing the residual strength of concrete structures post-fire [18,36]. Fire resistance refers to the duration a structural member can sustain applied loads and maintain its integrity under elevated temperatures [23,33,42]. In reinforced concrete (RC) elements, protecting the embedded steel reinforcement from thermal degradation is essential [1]. Traditional strategies include increasing member dimensions, adding additional concrete cover, or applying insulating coatings. While effective, such approaches can be material-intensive and less efficient in terms of weight and construction practicality.

An alternative strategy is the application of fire-resistant plaster using low thermal conductivity materials. For optimal performance, such materials should be non-combustible, non-toxic, and capable of delivering 2–3 h of protection with minimal thickness and added weight [51]. The National Building Code of India [39] permits the use of materials such as gypsum, vermiculite, and perlite for fire protection applications, further supporting the relevance of EV and EP in structural fire engineering.

The novel contribution of this study lies in the application of expanded vermiculite (EV) and expanded perlite (EP) as protective plaster coatings for reinforced concrete (RC) elements. While previous research has largely focused on incorporating these materials into concrete mix designs—typically as partial replacements for natural sand or cement to improve thermal performance—this study explores their external use as fire-protective layers [24,25,41,50]. EV, in particular, has demonstrated excellent heat resistance and thermal insulation properties [10,29,37,48]. Incorporating 5–25 % EV by weight into concrete has been shown to reduce thermal conductivity to between 0.23 and 0.50 W/mK [2], while similar use of EP can lower thermal conductivity to 0.16–0.35 W/mK.

A review by Assis Neto et al. [8] analyzed the impact of EV on the thermal properties of lightweight mortars. Replacing sand with EV was shown to reduce the thermal conductivity due to increased porosity. Durmuş & Topuz [13] examined foam concrete panels containing EP and polystyrene. In this study, the inclusion of EP improved the thermal insulation, achieving a thermal conductivity as low as 0.099 W/mK. Azimi et al. [9] investigated the post-fire properties of 3D printed concrete and it was shown that the inclusion of EP reduced the thermal conductivity and improved the post-fire structural integrity. Ulusu and Kurnuc Seyhan [57] evaluated the effect of EP aggregate plaster on RC structures exposed to high temperatures and found that it enhanced the thermal insulation, reducing the heat transfer to the underlying concrete. While expanded vermiculite and expanded perlite show promise in enhancing the fire resistance and thermal insulation of concrete materials, further research is needed to address their impact on mechanical properties, long-term durability, and performance under real fire conditions.

Several studies have explored the effects of incorporating expanded vermiculite (EV) and expanded perlite (EP) on the mechanical and thermal properties of concrete [5]. Replacing conventional constituents such as sand or cement with EV typically leads to increased porosity and reduced compressive strength due to the material's higher water absorption capacity [19]. For instance, replacing 20 % of cement with EP enhances thermal stability but reduces both compressive and flexural strength. Koksall et al. [30] observed that concrete mixes with cement-to-EV ratios of 1:4 and 1:8 exhibited compressive strength reductions of 29.6 % and 53.6 %, respectively, relative to control specimens. Concurrently, thermal conductivity decreased by 27.6 % and 58.1 %, respectively, due to the higher porosity induced by increased EV content [29]. Similar trends have been reported for EP, with up to 39 % increases in porosity when used as a sand replacement [48,52,56].

In the context of fire protection, EV and EP can be mixed with cement to form plaster coatings that significantly improve the fire performance of RC elements. Although research on this application is limited, studies have demonstrated promising results. Hodhod et al. [20] reported that an EV-cement plaster reduced thermal conductivity by 74 % compared to traditional sand-cement plaster. Formosa-Mitjans et al. [17] also observed thermal conductivity reductions with increasing vermiculite content, while Gencel et al. [19] showed that mortars incorporating EV as an aggregate achieved enhanced fire resistance. These findings are particularly significant given that fire temperatures can reach up to 1000°C.

El-Gamal et al. [14] found that cement pastes with 2.5–10 % EV retained substantial strength after exposure to 300–800°C for three hours, with optimal performance at 5 % EV. Abidi et al. [2] demonstrated that adding EP and EV to plaster composite panels improved thermal resistance. In another study, Hodhod et al. [20] observed that EV-cement plaster retained 64.3 % of its residual strength after exposure to 650°C for 30 min, compared to 50.4 % for sand-cement plaster. Similarly, El-Karmoty [15] reported that coating high-strength concrete columns with a 20 mm EP mortar layer increased residual load capacity by 26.5 % after exposure to 750°C for one hour. Liu et al. [35] tested foam concrete with EV as a sand replacement under heating up to 900°C; a 15 % EV replacement resulted in a 1.84 % strength reduction at 300°C, rising to 69.1 % at 900°C.

This study aims to investigate the use of EV and EP as fire-protective coatings on existing RC members, rather than solely as internal mix components. Vermiculite–Portland cement and perlite–cement coatings have been shown to significantly resist heat transmission [32], with perlite plasters offering four to six times the thermal resistance of traditional sand-based plasters, and vermiculite plasters offering a four-fold increase. Vermiculite is a hydrated magnesium–aluminium silicate mineral similar to mica, while perlite is formed from rapidly cooled volcanic glass. Both materials are non-combustible and have low thermal conductivity, making them ideal for improving fire performance. However, their high permeability also results in increased porosity and water absorption, which can negatively impact mechanical strength [43,54].

Despite these limitations, the integration of EV and EP into concrete or plaster formulations can be achieved with minimal changes to conventional batching or construction practices. Although the initial cost may be higher than traditional materials, long-term savings are possible due to reduced fire damage, improved structural resilience, and lower repair needs. Nonetheless, questions

remain regarding the long-term durability of EV and EP in concrete, particularly concerning moisture ingress, chemical attack, and freeze–thaw effects.

In conclusion, the literature supports the use of EV and EP to enhance the fire resistance of concrete, either through internal incorporation or as external coatings. Their beneficial effects are likely due to their low thermal expansion and conductivity, which help limit cracking and heat penetration, thereby preserving the structural integrity of RC elements under fire conditions. This paper builds on these findings by experimentally assessing the post-fire performance of RC beams coated with EV and EP plaster layers—a novel approach with limited prior investigation.

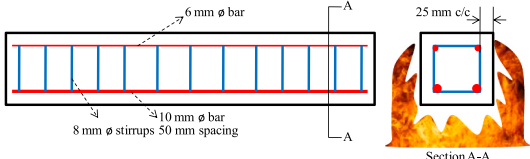
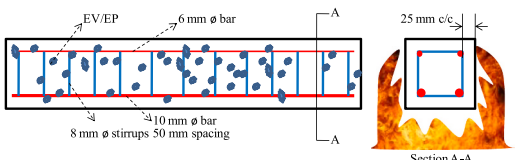
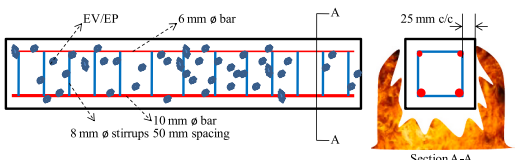
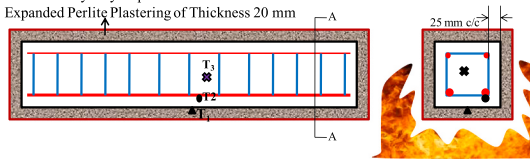
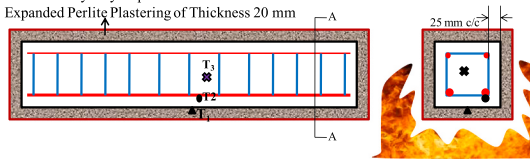
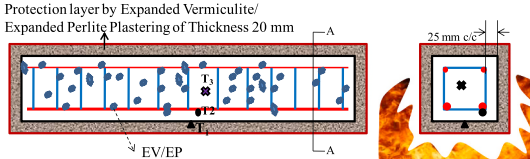
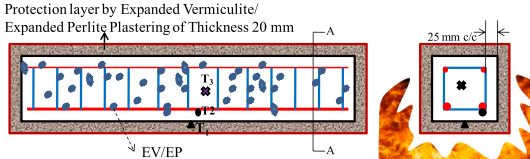
2. Experimental programme

An extensive experimental programme was conducted at the Structural Fire Testing Laboratory at Karunya University to examine the effects of expanded vermiculite (EV) and expanded perlite (EP) on the post-fire properties of reinforced concrete (RC) structures. The testing was carried out in two phases. In the first phase, 420 concrete cubes containing various levels of EV and EP were prepared and tested at elevated temperatures to determine the optimal replacement percentage. In the second phase, 42 RC beams, with EV and EP either incorporated into the concrete matrix or applied as a lightweight surface plaster, were exposed to high temperatures. Table 1 summarizes the details of the beam specimens in Phase 2. In the specimen designations, the first term indicates the concrete grade (either M20 or M50), and the second term specifies the type: reference mix without EV or EP (R), concrete mixes with EV (EV) or EP (EP), or mixes where EV or EP is applied as a surface plaster (EVC and EPC, respectively). Specimens designated as EV+EVC and EP+EPC feature both EV/EP within the concrete matrix and as an external plaster coating.

2.1. Materials

A total of 4 different grades of concrete were included in the test specimens in Phase 1, namely M20, M30, M40 and M50, and the mixes were designed in accordance with IS 10262 (2009). The contents of each grade is given in Table 2, and the mixes were designed to achieve a target slump of 100–125 mm. As stated before, a total of 420 concrete cubes were cast, each of which was 150 × 150 × 150 mm in size, as well as 42 beams, which were 700 mm in length and had a square cross-section which was

Table 1
Outline of the test programme.

Specimen designation	Schematic representation of Protective Methods	Duration of heating	No. of specimens
M20-R, M50-R		60, 90 and 120 min	06
M20-EV, M50-EV (for 5 % replacement only)		60, 90 and 120 min	06
M20-EP, M50-EP (for 2.5 % replacement only)		60, 90 and 120 min	06
M20-EVC, M50-EVC (EV as plastering only)		60, 90 and 120 min	06
M20-EPC, M50-EPC (EP as plastering only)		60, 90 and 120 min	06
M20-EV+EVC, M50-EV+EVC (Combination of mix and plastering)		60, 90 and 120 min	06
M20-EP+EPC, M50-EP+EPC (Combination of mix and plastering)		60, 90 and 120 min	06

200 × 200 mm. The specimens were cured for 28 days by covering/spraying them with water to simulate real practice. They were then dried thoroughly prior to conducting elevated temperature tests.

The basic mix design for the concrete comprised grade 53 Ordinary Portland Cement (OPC), with a specific gravity of 3.15, in accordance with the specifications given in IS:12269 (2013). River sand which was available locally was used as the fine aggregate, and this was found to have a specific gravity of 2.70, conforming with the materials characterised as zone-II as given in IS:383 (2016). The sand was then dried before being used, to avoid bulking during mixing. The coarse aggregate comprised locally available granite with a maximum dimension of 20 mm. The specific gravity of the coarse aggregate was found to be 2.8. Potable water was used for mixing and curing.

Within each grade of concrete examined (M20-M50), different levels of EV and EP were added in place of the fine aggregate, as given in Table 3. The replacement was between 2.5 % and 10 % by weight for the EV and between 2.5 % and 10 % by volume for the EP, as EP is very lightweight. In the mix designations given in the table, the second term describes the replacement percentage of EV or EP that were included in that mix, in place of the sand (i.e. EV0 is a mix without any EV, EV2.5 had 2.5 % by weight of EV added in place of the same amount of fine aggregate, etc.). The EV and EP minerals were obtained from local suppliers in India and had a specific gravity of 0.22 and 0.20, respectively, as well as a maximum dimension of 5 mm. These mixes were prepared using the same materials as the concrete previously described, that is OPC, coarse aggregate, fine aggregate and a varying amount of EV or EP. To study the post-fire performance of RC beams, the proposed protection techniques as outlined in Table 1 were applied to the RC beams only. There cube tests were to measure the actual compressive strength of specimens cast with and without EP or EV, and both heated and unheated conditions were included.

As stated before, one of the key aims in this work is to examine the influence of applying EP or EV, mixed with cement into a plaster, externally to the surface of RC beams, to improve the thermal performance. As such, 24 of the 42 beams tested were coated in these materials using the mix proportions given in Table 4. OPC was used for the cement and the thickness of the plaster as applied to the beams was 20 mm. A large number of trials using different mix ratios were tested to achieve the optimum bond and heat insulation properties.

2.2. Test methodology

As stated before, the experimental programme was conducted in two phases comprising (i) a series of 420 compression tests on 150 × 150 mm cubes to optimise the replacement percentage for the of EV or EP and (ii) a total of 42 structural fire tests on RC beams, as given in Table 5. The following subsections provide more information on the methodology of testing for each of these phases.

2.2.1. Compression tests

The compression test specimens were heated in an electric furnace as shown in Fig. 1, in accordance with the standard fire curve given in ISO 834 [22] for durations of 30, 45, 60 or 90 mins. Following exposure to the desired temperature for required length of time, the specimens were removed from the furnace and then allowed to naturally cool down to room temperature before being tested using a concrete cube crushing machine.

2.2.2. Beam tests

Each of the 42 RC beams which were examined had identical geometries but different material properties. Following casting, beams were cured for 28 days, during which they were sprayed with water. The specimens were fully dried before each test commenced. The members were reinforced with 2 longitudinal tensile reinforcing bars, each 10 mm in diameter (ϕ) and these were placed 25 mm from the bottom (tensile) surface of the beams. There were also two reinforcing bars with a diameter of 6 mm employed as hanger bars and 8 mm diameter shear stirrups at 50 mm intervals along the beam lengths. The beams were heated in an electric furnace (shown in Fig. 1) with electrical heating coils. The beam was heated from 3 sides, the unheated portion was the compression side of the beam, and the exposed portion was the tension side. The maximum temperature at which the furnace can operate was 1200°C. The specimens were heated in accordance with standard fire curve [22] as shown in Fig. 2, up to 60 min (corresponding to 718°C), 90 min (976°C) and 120 min (1029°C). After the beams were exposed to the target temperatures and duration, the furnace was switched off, and the specimens were removed and allowed to naturally cool to normal temperature.

Table 2
Mix designs.

Material	Unit	Grade			
		M20	M30	M40	M50
Water/cement ratio		0.58	0.51	0.36	0.32
Water	kg/m ³	192.21	192.21	152.9	152.9
Cement	kg/m ³	323.9	384.1	413.9	449.9
Coarse aggregate	kg/m ³	873.6	820.2	1157.2	1145.3
Fine aggregate	kg/m ³	1071.4	1072.9	802.9	770.8
Admixture (Super-Plasticizer)	kg/m ³	-	-	5.6	5.6

Table 3

Details of Mix Proportion with the replacement of EV and EP in fine aggregate.

Mix	Fine aggregate (kg/m ³)	Expanded Vermiculite (kg/m ³)	Mix	Fine aggregate (kg/m ³)	Expanded Perlite/ Fine aggregate (by volume)
M20-EV0	1070.00	0	M20-EP0	1070.00	0
M20-EV2.5	1043.25	26.75	M20-EP2.5	1043.25	2.5
M20-EV5	1016.50	53.50	M20-EP5	1016.50	5
M20-EV7.5	989.78	80.25	M20-EP7.5	989.78	7.5
M20-EV10	963.00	107.00	M20-EP10	963.00	10
M30-EV0	1073.00	0	M30-EP0	1073.00	0
M30-EV2.5	1046.18	26.82	M30-EP2.5	1046.18	2.5
M30-EV5	1019.35	53.65	M30-EP5	1019.35	5
M30-EV7.5	992.53	80.47	M30-EP7.5	992.53	7.5
M30-EV10	965.70	107.30	M30-EP10	965.70	10
M40-EV0	803.00	0	M40-EP0	803.00	0
M40-EV2.5	782.93	20.07	M40-EP2.5	782.93	2.5
M40-EV5	762.85	40.15	M40-EP5	762.85	5
M40-EV7.5	742.78	60.22	M40-EP7.5	742.78	7.5
M40-EV10	722.70	80.30	M40-EP10	722.70	10
M50-EV0	771.00	0	M50-EP0	771.00	0
M50-EV2.5	751.73	19.27	M50-EP2.5	751.73	2.5
M50-EV5	732.45	38.55	M50-EP5	732.45	5
M50-EV7.5	683.18	87.82	M50-EP7.5	683.18	7.5
M50-EV10	693.90	77.10	M50-EP10	693.90	10

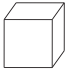
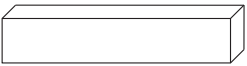
Table 4

Details of concrete mix design for the EV/EP plaster.

Mix proportions (relative to the weight of the cement)	EV based plaster	EP based plaster
Cement	1.0	1.0
EV	4.0	0.0
EP	0.0	4.0
Water	0.7	0.7

Table 5

Details of the test specimens.

Test group	Specimen geometry (mm)	Grade	Duration of heating (min)	No. of test specimens
Compressive strength tests	 150 × 150 × 150	M20, M30, M40, M50	30, 45, 60, 90, 120	420
Structural Fire tests on RC beams	 700 × 200 × 200 700 × 200 × 200	M20, M50 (with protective methods- Table 1)	0, 60, 90 and 120	42

3. Concrete compressive strength following exposure to elevated temperature – results and analysis

This section presents the compressive strength of concrete, with and without EV or EP present in the mix, at ambient temperature and following exposure to different durations of elevated temperature. This behaviour is important to fully assess and understand before assessing member behaviour, as in [Section 5](#).

3.1. Ambient temperature

[Figs. 3 and 4](#) present the compressive strength of concrete for different grades of concrete with varying levels of EV and EP content, respectively. It is clear that, in general, the compressive strength is generally reduced with increasing dosages of EP or EV in the design mix, compared with just sand as the fine aggregate (as is the case for the EV0 and EP0 specimens). Firstly, with reference to the data in



Fig. 1. Electrical furnace.

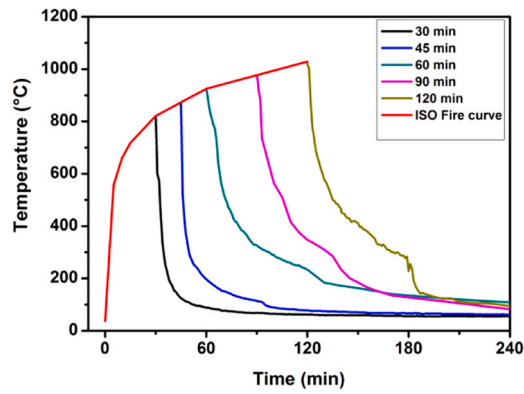


Fig. 2. Heating-cooling regime.

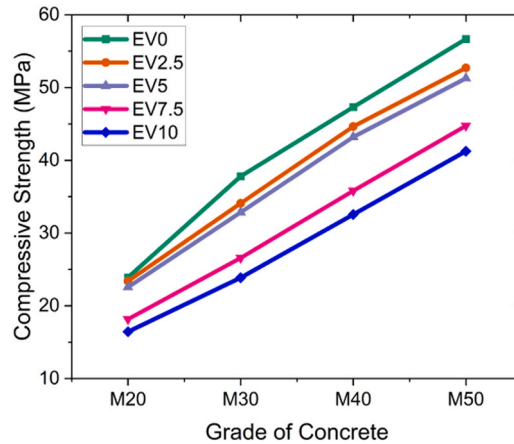


Fig. 3. Compressive strength of concrete containing EV in place of sand.

Fig. 3 for the specimens with EV, the compressive strength values at 28 days of for the M20 grade concrete with 0, 2.5, 5.0, 7.5 and 10 % EV content were 23.9, 23.4, 22.6, 18.2 and 16.4 MPa, respectively. Therefore, the compressive strength of M20-EV10 was 32 % lower than for M20-EV0. For the strongest grade of concrete examined, M50, the corresponding strengths were 56.5, 52.7, 51.2, 44.8, and 41.3 MPa for specimens with 0, 2.5, 5.0, 7.5 and 10 % EV content, respectively, and therefore M50-EV10 had a compressive strength which was 27 % lower than the equivalent value for M50-EV0. This reduction in strength is as expected, owing to the greater porosity and therefore increased water absorption of concrete with EV, compared with natural sand. The inclusion of EV in the matrix decreases the unit weight of concrete. In the case of vermiculite mortars, this tendency for the compressive strength to reduce is due to the porous, soft nature of the matrix. The weaker aggregate offers less resistance to crack propagation, consequently causing a

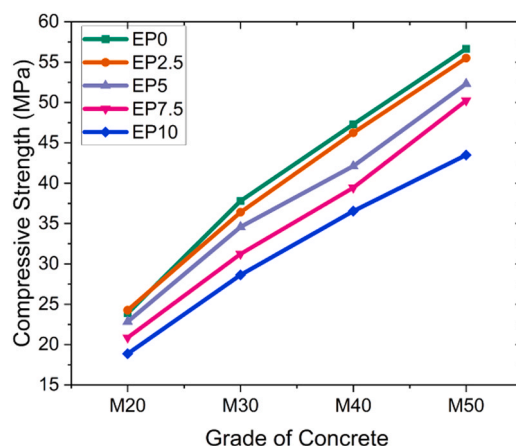


Fig. 4. Compressive strength of concrete containing EP in place of sand.

reduction of the load-carrying capacity. It has been suggested that the reason for the reduction in compressive strength might be related not only to the higher porosity but also to the greater water demand during the mixing process when EV is present, to complete the hydration process [4].

Similarly, the data presented in Fig. 4 for the specimens containing EP illustrates a similar trend to those with EV. Accordingly, the compressive strength of concrete containing EP reduces as the EP content increases, again owing to the greater porosity of the EP relative to natural sand. The compressive strength values at 28 days for M20 grade concrete with 0, 2.5, 5.0, 7.5 and 10 % EP content were 23.9, 24.27, 22.84, 20.87 and 18.87 MPa, respectively. This reduction was found to be similar for the other grades of concrete examined, containing EP. For the M50 grade concrete, the corresponding strengths were 56.57, 55.5, 52.32, 50.24, and 43.5 MPa for specimens with 0–10 % EV content, respectively, and therefore M50-EP10 had a compressive strength which was 23.29 % lower than the equivalent value for M50-EP0.

It is important to note that replacing conventional aggregates with expanded vermiculite (EV) or expanded perlite (EP) can significantly reduce compressive strength. For instance, concrete with 25 % sand replacement by EV has shown a marked strength reduction, suggesting unsuitability for high-performance applications [11]. Similarly, incorporating EP also results in decreased compressive strength, with the extent of reduction depending on the replacement level [49]. To mitigate this impact on structural performance, an optimum replacement percentage must be identified to balance thermal benefits with acceptable strength levels—potentially aided by supplementary materials such as fly ash. As lightweight aggregates, perlite and vermiculite are highly porous, which can enhance fire resistance. Therefore, this study seeks to determine an optimum level of lightweight aggregate replacement that maintains the target compressive strength. Being mineral-based and lightweight, these aggregates do not increase the self-weight of the structural section, and under non-fire conditions, their use has negligible impact on design considerations.

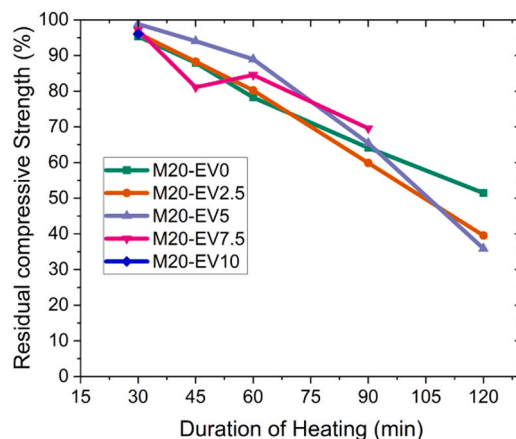


Fig. 5. Residual post-fire compressive strength of M20 concrete with EV included in the mix design.

3.2. Following exposure to elevated temperature

3.2.1. Concrete containing EV

This section presents the results of compression tests on concrete cubes with varying levels of EV, following exposure to elevated temperatures. The residual compressive strength was measured after cooling, and results are shown in Figs. 5–8, grouped by concrete grade. The y-axis displays the percentage of residual compressive strength for each specimen, shown on the x-axis. As expected, compressive strength decreases with longer exposure to high temperatures for all mix designs. However, the trends observed in these tests differ notably from those at ambient temperature, as shown in Fig. 3. For each temperature exposure duration (e.g., 30 min), the presence of EV in the mix generally enhances residual strength compared to EV-free samples (EV0) across all grades tested. Specifically, specimens containing 2.5 %, 5 %, 7.5 %, or 10 % EV showed a slight increase in compressive strength after up to 90 min of heating. The early-stage strength gain can be attributed to an additional hydration process in the cement paste, known as internal autoclaving. This is facilitated by the porous nature of EV, which absorbs, retains, and gradually releases water, thereby enhancing internal curing. At lower temperatures, this internal curing effect improves performance and reduces microcracking under thermal stress. However, at elevated temperatures, the porous structure of EV may contribute to increased degradation due to the formation of additional voids and microcracks [35].

Fig. 8 illustrates the variation in residual compressive strength for M50-grade concrete across the different mixes. For 30 min of heating, residual strength values for M50-EV0, M50-EV2.5, M50-EV5, M50-EV7.5, and M50-EV10 were 107.4 %, 108.8 %, 115.2 %, 113.3 %, and 105.6 % of their unheated counterparts, respectively, consistent with findings from other studies (e.g., [26,59]). This strength increase relative to unheated specimens may result from the hydration of anhydrous cementitious materials due to water migration within the pores, enhancing bond properties in the cement paste. Additionally, heating to temperatures up to 300 °C appears to improve mechanical properties due to water evaporation and closer contact of cement gel layers, increasing Van der Waals forces [12,21,26].

A notable strength reduction occurred in all concrete mixtures (M20–M50) after 60 min of heating. This decline is attributed to inner cracking due to dehydration and pressure from physically bound water. Prolonging exposure from 60 min (925 °C) to 120 min (1029 °C) resulted in significant further strength loss. At 120 min of heating, the residual compressive strengths for M50-EV0, EV2.5, EV5, EV7.5, and EV10 were 35.54 %, 45.24 %, 51.14 %, 35.84 %, and 0 % (spalled), respectively, of their unheated values. Another notable observation from the results is that a 5 % replacement of river sand with EV in the concrete mix demonstrated the best performance in terms of strength retention following exposure to elevated temperatures. After 60 min of heating, the residual compressive strength of M20-EV5 increased by 10.7 % compared to the reference mix (M20-EV0), while M50-EV5 showed an even greater improvement of 21.4 % compared to M50-EV0. This superior performance can be attributed to the granular structure of EV, which contains numerous air voids acting as effective thermal insulators. These voids mitigate the detrimental effects of high temperatures on the concrete specimens. The porous nature of EV contributes positively to maintaining residual strength after exposure to elevated temperatures, even though it slightly reduces the compressive strength at ambient temperatures, as previously discussed.

3.2.2. Concrete containing EP

This section presents the results of compression tests on concrete cubes containing various levels of EP, after exposure to elevated temperatures, as shown in Fig. 2. Following cooling, the residual strength of the concrete was determined. The results, presented in Figs. 9–12 for different concrete grades, indicate that compressive strength generally decreased with longer exposure to elevated temperatures. However, notable differences were observed in the trends compared to those presented in Fig. 4 (ambient temperature) and Figs. 5–8 (concrete containing EV). Across all cases, concrete mixes with a 2.5 % replacement of sand with EP (denoted as EP2.5) exhibited superior residual strength compared to the reference mix (EP0) after all levels of temperature exposure. For most grades, a slight increase in compressive strength was observed for specimens with 2.5 % EP, while mixes with 5 % EP showed a more

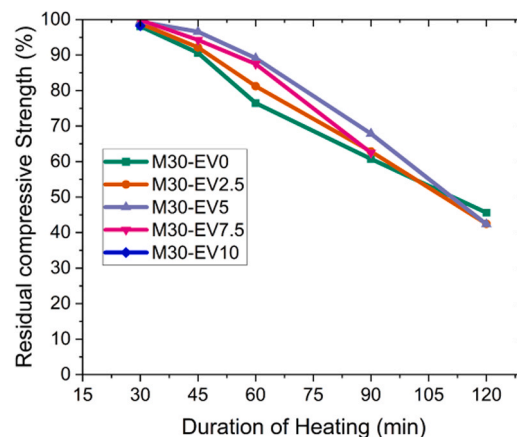


Fig. 6. Residual post-fire compressive strength of M30 concrete with EV included in the mix design.

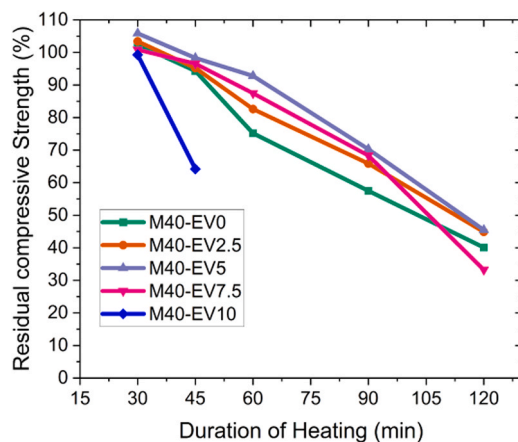


Fig. 7. Residual post-fire compressive strength of M40 concrete with EV included in the mix design.

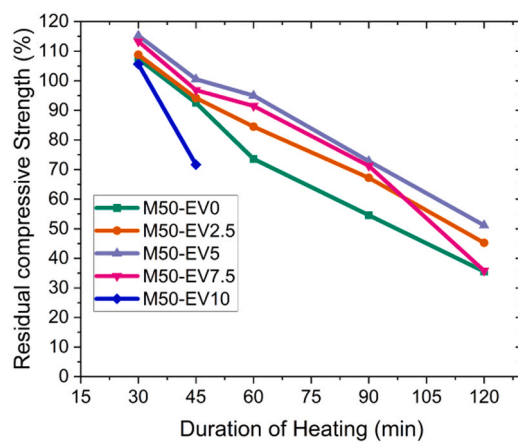


Fig. 8. Residual post-fire compressive strength of M50 concrete with EV included in the mix design.

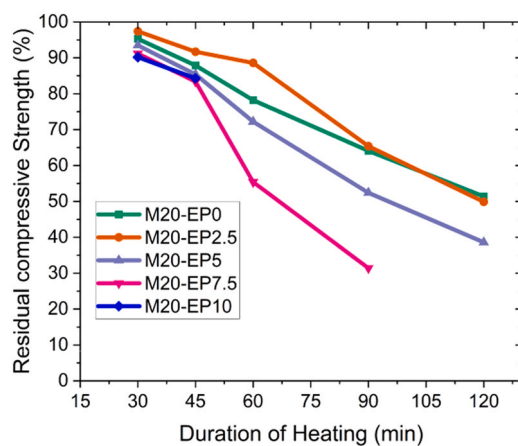


Fig. 9. Residual post-fire strength of M20 concrete with EP included in the mix design.

pronounced improvement, particularly in higher-grade concretes (M40 and M50). In contrast, replacement levels exceeding 5 % EP led to spalling, rendering these mixes ineffective.

The behaviour trends were consistent across all concrete grades. For example, the percentage residual compressive strengths of

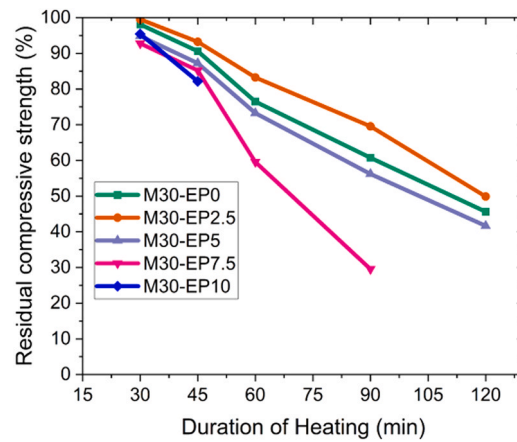


Fig. 10. Residual post-fire strength of M30 concrete with EP included in the mix design.

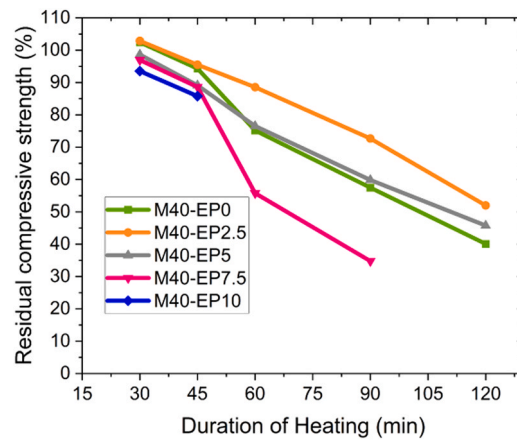


Fig. 11. Residual post-fire strength of M40 concrete with EP included in the mix design.

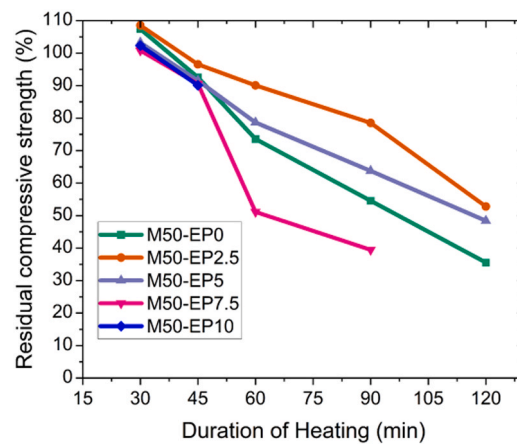


Fig. 12. Residual post-fire strength of M50 concrete with EP included in the mix design.

M50 concrete exposed to 30 min of heating were 107.4 %, 108.5 %, 103.3 %, 100.8 %, and 102.3 % for mixes containing 0 %, 2.5 %, 5 %, 7.5 %, and 10 % EP, respectively. After 120 min of heating, the corresponding values were 35.5 %, 52.8 %, 48.4 %, 0 % (spalled), and 0 % (spalled). Another notable observation from the results is that a 2.5 % replacement of river sand with EP in the concrete mix demonstrated the best performance in terms of strength retention following exposure to elevated temperatures. Notably, after 60 min

of heating, the residual compressive strength increased by approximately 10.4 % for M20-EP5 specimens compared to the reference mix (M20-EP0) and by 16.5 % for M50-EP5 compared to M50-EP0. This reduction in strength loss can be attributed to the granular and lightweight nature of EP, which contains numerous air voids. These voids act as effective insulators, mitigating the detrimental effects of elevated temperatures on concrete specimens.

3.2.3. Comparative analysis of EV and EP on high-temperature performance

Expanded vermiculite (EV) and expanded perlite (EP) are lightweight aggregates commonly used to improve the high-temperature performance of concrete. While both enhance thermal insulation, their effects on mechanical properties under elevated temperatures differ due to their distinct physical and chemical characteristics. Concrete incorporating EV has demonstrated notable thermal stability. Studies show that replacing 5 % of cement with EV can improve residual strength after exposure to temperatures up to 800 °C, attributed to its low thermal conductivity and ability to limit microstructural degradation under heat [14]. The layered silicate structure of EV helps form a denser microstructure, reducing crack propagation and preserving the cement matrix during thermal cycling.

EP also offers excellent thermal insulation, significantly lowering the thermal conductivity of concrete [8]. However, its inclusion often leads to a reduction in compressive strength, especially at higher replacement levels. For example, replacing 40 % of natural aggregate with EP can result in considerable strength loss, despite improved thermal resistance [38]. At temperatures above 400 °C, EP's porous structure can exacerbate microcracking, compromising mechanical integrity.

From a cost perspective, partial replacement of fine aggregate with 2.5 %–10 % EV or EP increases concrete costs by 4 %–8 % per m^3 , offering enhanced thermal and fire resistance. When M-sand is replaced with EP at the same levels, costs can rise by 8 %–30 % per m^3 , but the trade-off in terms of improved insulation and lightweight properties is advantageous for applications in fire-prone environments and post-fire repair. Regarding plastering, M-sand plaster remains the most economical due to its availability and standard application methods. EV plaster, by contrast, is substantially more expensive—typically 5–12 times the cost of M-sand plaster—due to the specialised nature of the material and the need for skilled labour. EP plastering is similarly costly, ranging from 4–11 times more expensive depending on labour rates and mix proportions.

4. Beam behaviour following exposure to elevated temperature – results and analysis

This section presents the results and analysis of the experimental investigation into the residual structural performance of reinforced concrete (RC) beams exposed to elevated temperatures and subsequent cooling. The programme comprised a total of 42 RC beams with various material configurations, as outlined in Table 1, which can be categorised into the following three groups:

- (1) RC beams with EV or EP incorporated into the concrete mix (12 tests);
- (2) RC beams with EV or EP plaster applied externally (12 tests); and
- (3) RC beams with EV or EP both incorporated in the concrete mix and applied externally as a protective plaster (12 tests).

Fig. 13 provides a schematic representation of an RC beam coated with a layer of EV or EP plaster. The discussion encompasses the influence of temperature exposure on key structural parameters, including the (i) load-deflection response, (ii) cracking behaviour, (iii) ultimate load capacity, (iv) temperature distribution through the section, (v) yield strength of reinforcement, and (vi) failure modes. Comparisons are made between protected and unprotected beams constructed with different concrete grades (M20 and M50), highlighting the efficacy of protective measures such as embedded materials (EV and EP) and external plaster coatings (EVC and EPC). The findings provide a comprehensive understanding of the thermal and structural interactions in fire-affected RC beams, with implications for designing fire-resilient structural systems.

4.1. Load-deflection behaviour

Figs. 14–16 illustrate the load-deflection responses for M20 concrete beams exposed to 60, 90, and 120 min of heating, respectively, while Figs. 17–19 present the corresponding results for M50 concrete beams. A key observation across all tests is that the

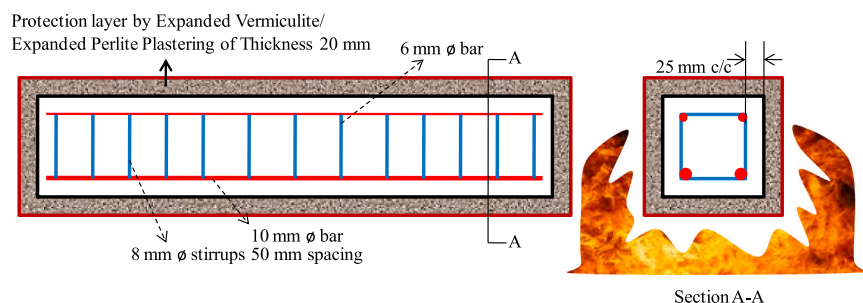


Fig. 13. Schematic of an RC beam with a layer of protective EV or EP plaster.

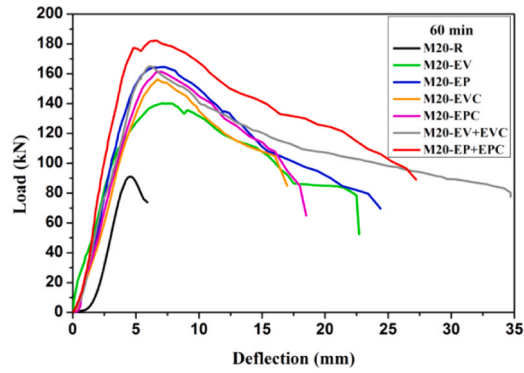


Fig. 14. Load-deflection behaviour of RC beams made using M20 concrete exposed to 60 min of heating.

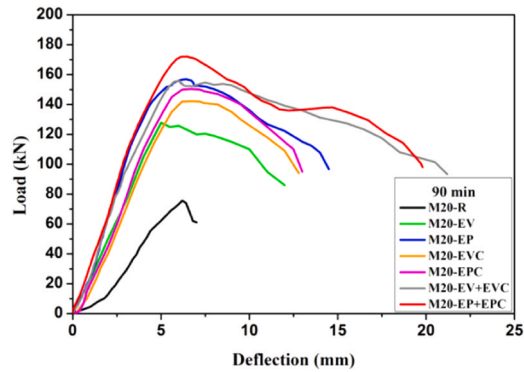


Fig. 15. Load-deflection behaviour of RC beams made using M20 concrete exposed to 90 min of heating.

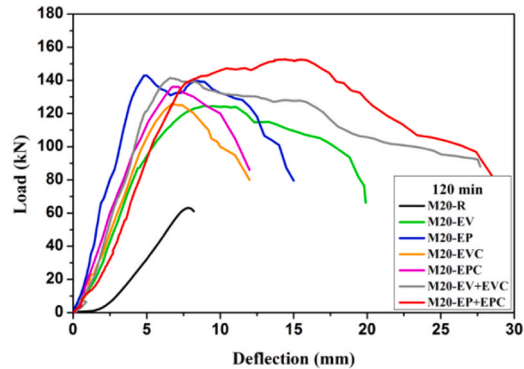


Fig. 16. Load-deflection behaviour of RC beams made using M20 concrete exposed to 120 min of heating.

reference beams without EP or EV consistently exhibited the poorest performance after fire exposure. These beams demonstrated the lowest ultimate loads, failed earlier, and exhibited inferior behaviour throughout the loading stages, from initial cracking to failure. In contrast, beams incorporating EP (either in the concrete mix or externally as a plaster) generally outperformed those with EV, a finding that contrasts with the compression test results. Beams with both EP in the mix and as a protective plaster achieved the highest ultimate loads and exhibited the best overall performance. These specimens displayed excellent ductility in the softening branch, particularly after peak load. All beams incorporating either EP or EV, whether in the concrete matrix or applied externally, exhibited favourable performance. Their load-deflection responses were characterized by robust elastic behaviour, followed by a gradual softening response post-peak, reflecting a ductile failure mode. The softening branch was less steep for beams subjected to higher heating durations, indicating improved post-fire residual strength at elevated temperatures. Notably, beams exposed to prolonged heating (120 min) retained a significant proportion of their strength compared with those heated for shorter durations (60 min). This highlights the critical role of temperature distribution across the beam's cross-section, which is influenced by factors such as the water-to-cement

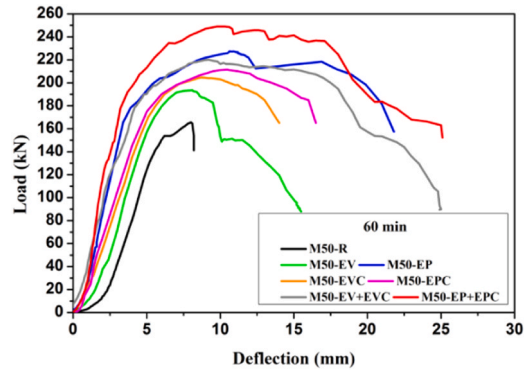


Fig. 17. Load-deflection behaviour of RC beams made using M50 concrete exposed to 60 min of heating.

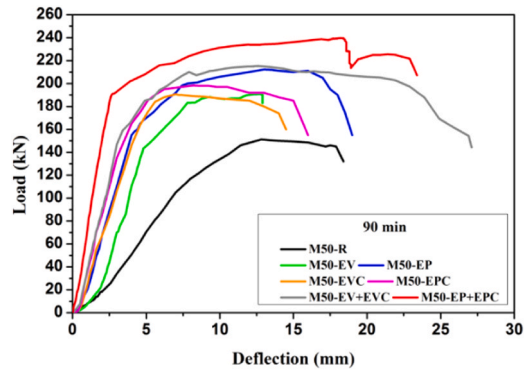


Fig. 18. Load-deflection behaviour of RC beams made using M50 concrete exposed to 90 min of heating.

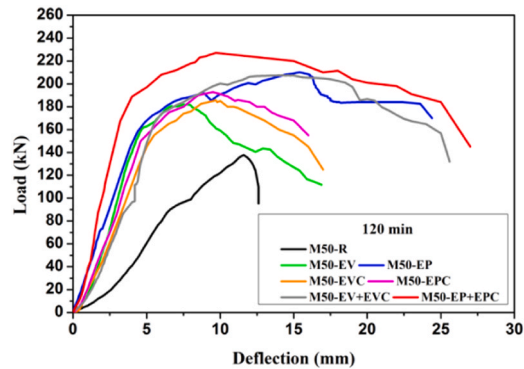


Fig. 19. Load-deflection behaviour of RC beams made using M50 concrete exposed to 120 min of heating.

ratio, concrete density, and thermal conductivity [7,47,55].

As shown in Figs. 14–16, the load-deflection responses of both protected (M20-EV, M20-EP, M20-EVC, M20-EPC, M20-EV+EVC, and M20-EP+EVC, with plaster coatings) and unprotected (M20-R) M20 RC beams exhibited tensile cracking during the initial stages of loading, ultimately failing through concrete crushing before the steel reinforcement reached its yield strength. Tensile cracks in the M20 beams developed at load levels ranging from 47–76 kN, 54–105 kN, and 53–113 kN after exposure durations of 60, 90, and 120 min, respectively. In comparison, tensile cracking in M50 beams occurred at lower load ranges of 34–42 kN, 38–45 kN, and 46–53 kN for the same heating durations, as shown in Figs. 17–19. Despite this, M20 beams exhibited a more brittle response than M50 beams. For the M20 beams heated for 60 min, the peak loads achieved by the unprotected (M20-R) and fully protected (M20-EP+EVC) specimens were 91.14 kN and 182.1 kN, respectively. The protective plaster effectively mitigated the detrimental effects of elevated temperatures, preserving the yield strength of the steel reinforcement. Figs. 17–19 also demonstrate the load-deflection responses for M50 RC beams, both protected (M50-EV, M50-EP, M50-EVC, M50-EPC, M50-EV+EVC, and M50-EP+EVC) and unprotected (M50-R).

Unlike the M20 beams, the M50 specimens showed significant plastic deformation following tensile cracking, with failure occurring through flexural yielding of the steel reinforcement. The enhanced ductility and strength retention in the M50 beams highlight the superior post-fire performance of higher-strength concrete.

4.2. First cracking

The load at first cracking provides critical insights into the residual flexural strength of beams after exposure to elevated temperatures. The results indicate that the initiation of the first crack was influenced primarily by the compressive strength of the concrete, the water-to-cement (w/c) ratio, and the yield strength of the steel reinforcement, which are key factors governing the rate of strength reduction. For the reference RC beams (M20-R and M50-R), flexural tensile cracks originated at the mid-span region and progressively widened as the applied load increased, leading to flexural failure. However, for beams exposed to 60 min of heating, the first crack still initiated at mid-span, but inclined cracks developed near the supports as the load increased. This change in failure pattern was more pronounced in M20-grade beams than in M50-grade beams. Following 120 min of heating, vertical cracks appeared initially, followed by diagonal cracks, and concrete crushing occurred prior to failure. The failure mode progressively shifted from flexural to shear, often accompanied by bond failure.

The effect of heating duration on first crack loads P_{cr} and ultimate loads P_{ul} is summarized in Tables 6 and 7, respectively, where the subscripts of each term describe the duration of heating, while Table 8 presents the first crack load as a percentage of the ultimate load for the M20 and M50 RC beams. As heating duration increased, the beams exhibited greater rigidity, limiting the development of flexural cracking. For the M20 beams, the ratio of first crack load to ultimate load was relatively high for specimens heated for 120 min, highlighting a pronounced shift in failure mode from flexure to shear. Reduced flexural capacity results from the degradation of concrete and reinforcing qualities caused by high temperatures [6]. The microstructure of the concrete deteriorates and the bond between the concrete and reinforcement degrades at high temperatures, thus reducing the concrete's resistance to bending capacity [16]. Furthermore, the aggregate interlock which is essential for shear resistance was weakened by micro-cracking and spalling caused by high temperatures [34]. Because of the combined reduction in both flexural and shear capacities, the failure mode of the beam changes from a ductile flexural failure to a more brittle shear failure, with the shear resistance being specifically affected. For example, after 60 min of heating, the first crack load for the M20-EP+EPC beam was 42.1 % of its ultimate load, while the corresponding value for the M50-EP+EPC beam was just 13.84 %. These differences reflect the impact of concrete grade and heating duration on the residual flexural behaviour of RC beams.

Concrete with higher water content, such as M20, exhibited a greater reduction in strength during heating compared to M50 concrete. For the M20 beams, the difference between the peak load and the first crack load was relatively low due to the deterioration of the steel-concrete bond [58]. This difference further reduced with increased heating duration. Conversely, for M50 beams, the gap between the peak and first crack loads remained more pronounced, though it also decreased after prolonged heating. After 120 min of exposure, most specimens showed extensive cracking, with the severity influenced by heating duration, concrete porosity, and water content.

4.3. Ultimate capacity

The ultimate load-carrying capacities P_{ul} of the M20 and M50 RC beams exposed to various durations of heating (i.e. $P_{ul,0 \text{ mins}}$, $P_{ul,60 \text{ mins}}$, $P_{ul,120 \text{ mins}}$ and $P_{ul,180 \text{ mins}}$) are presented in Table 7. The results reveal that increasing the heating duration significantly reduced the load-carrying capacity of the beams, with the effect more pronounced for M20 concrete than for M50. For the protected M20 beams (M20-EP+EPC), the strength retained were 87.1 %, 82.3 %, and 73.2 % following 60, 90, and 120 min of heating, respectively. In contrast, the unprotected M20-R beams showed retentions of 43.6 %, 36.2 %, and 30.2 % for the same heating durations. Similarly, for M50 beams, the residual strength for the protected M50-EP+EPC were 97 %, 94.3 %, and 91.9 % compared to 68.4 %, 62.2 %, and 56.4 % for the unprotected M50-R beams over the same durations.

Table 6
First cracking load P_{cr} of RC beams following exposure to elevated temperature.

	$P_{cr,0 \text{ min}}$	$P_{cr,60 \text{ min}}$	$P_{cr,60 \text{ min}}/P_{cr,0 \text{ min}}$	$P_{cr,120 \text{ min}}$	$P_{cr,120 \text{ min}}/P_{cr,0 \text{ min}}$	$P_{cr,180 \text{ min}}$	$P_{cr,180 \text{ min}}/P_{cr,0 \text{ min}}$
M20-R	39.7	47.1	1.19	54.7	1.38	53.5	1.35
M20-EV	39.7	73.7	1.86	95.7	2.41	113.2	2.85
M20-EP	39.7	81.5	2.05	113.6	2.86	120.2	3.03
M20-EVC	39.7	78.8	1.99	102.7	2.58	110.5	2.78
M20-EPC	39.7	73.6	1.85	102.4	2.58	112.5	2.83
M20-EV+EVC	39.7	78.1	1.97	104.2	2.62	112.6	2.83
M20-EP+EPC	39.7	76.7	1.93	105.1	2.65	113.4	2.86
M50-R	29.3	42.0	1.43	45.0	1.54	46.0	1.57
M50-EV	29.3	36.7	1.25	41.2	1.41	48.9	1.67
M50-EP	29.3	39.3	1.34	47.0	1.61	53.7	1.84
M50-EVC	29.3	37.1	1.27	39.5	1.35	47.6	1.63
M50-EPC	29.3	35.4	1.21	38.2	1.30	46.2	1.58
M50-EV+EVC	29.3	36.1	1.23	38.1	1.30	46.5	1.59
M50-EP+EPC	29.3	34.5	1.18	38.6	1.32	48.1	1.64

Table 7Ultimate loads P_{ul} of RC beams following exposure to elevated temperature.

	$P_{ul,0 \text{ min}}$	$P_{ul,60 \text{ min}}$	$P_{ul,60 \text{ min}} / P_{ul,0 \text{ min}}$	$P_{ul,120 \text{ min}}$	$P_{ul,120 \text{ min}} / P_{ul,0 \text{ min}}$	$P_{ul,180 \text{ min}}$	$P_{ul,180 \text{ min}} / P_{ul,0 \text{ min}}$
M20-R	209.1	91.1	0.44	75.6	0.36	63.1	0.30
M20-EV	209.1	140.1	0.67	127.7	0.61	124.6	0.60
M20-EP	209.1	164.5	0.79	156.7	0.75	142.9	0.68
M20-EVC	209.1	156.2	0.75	142.1	0.68	125.8	0.60
M20-EPC	209.1	161.5	0.77	150.3	0.72	136.1	0.65
M20-EV+EVC	209.1	165.0	0.79	155.7	0.74	141.5	0.68
M20-EP+EPC	209.1	182.1	0.87	172.1	0.82	153	0.73
M50-R	244.1	165.5	0.68	151.2	0.62	137.8	0.56
M50-EV	244.1	193.5	0.79	190.9	0.78	181.9	0.75
M50-EP	244.1	227.4	0.93	212.7	0.87	210	0.86
M50-EVC	244.1	204.6	0.84	190.6	0.78	185.6	0.76
M50-EPC	244.1	211.5	0.87	198.4	0.81	192.8	0.79
M50-EV+EVC	244.1	220.1	0.90	215.3	0.88	207.5	0.85
M50-EP+EPC	244.1	237.1	0.97	230.2	0.94	227.8	0.92

Table 8

First crack load as percentage of ultimate load for RC beams with M20 and M50 concrete.

Duration of heating (min)	First crack load as percentage of ultimate load (%)						
	M20-R	M20-EV	M20-EP	M20-EVC	M20-EPC	M20-EV+EVC	M20-EP+EPC
60	51.68	52.61	49.57	50.48	45.60	47.35	42.14
90	72.32	74.91	72.51	72.24	68.13	66.92	61.07
120	84.71	90.85	84.11	87.87	82.62	79.54	74.12
	M50-R	M50-EV	M50-EP	M50-EVC	M50-EPC	M50-EV+EVC	M50-EP+EPC
60	25.38	18.96	17.28	18.14	16.75	16.41	13.84
90	29.76	21.59	22.10	20.75	19.26	17.67	16.12
120	33.38	26.86	25.59	25.67	23.97	22.40	21.11

Protected M20 beams incorporating EV or EP (M20-EV and M20-EP) demonstrated significant improvements, with load-carrying capacities increasing by 53 % and 80 %, respectively, after 60 min of heating. When a protective layer was also applied (M20-EV+EVC and M20-EP+EPC), these increases rose to 81 % and 99.8 %, respectively. Notably, the ultimate load of the M20-EP+EPC beam increased by 142 % compared to M20-R after 120 min of heating. For M50 beams, incorporating EV or EP resulted in load-carrying capacity increases of 17 % and 37 % for M50-EV and M50-EP, respectively, compared to M50-R after 60 min of heating. With an additional protective layer (M50-EV+EVC and M50-EP+EPC), these increases were 32 % and 50 %, respectively. The M50-EP+EPC beam exhibited the highest improvement, with a 65 % increase in flexural capacity compared to M50-R after 120 min of heating. The external protective layer effectively mitigated the negative impact of elevated temperatures on the steel reinforcement, while the EP component contributed to retaining the compressive strength of the concrete, delaying the onset of failure. These findings underscore the benefits of incorporating EP and EV in both the mix design and as external coatings to enhance the residual capacity of RC beams exposed to high temperatures.

4.4. Temperature distribution in the protected RC beams

The increase in temperature in the steel rebars and concrete was measured by employed 'K' type thermocouples in the beams at the following locations, and as shown in Fig. 20.

- On the surface of the specimens (T_1);
- On the main rebars at the mid-section of the beam (T_2) 20 mm from the exposed surface; and
- In the inner core of the specimen 100 mm from the bottom of the beam (T_3).

The primary objective was to determine the critical failure temperature for both protected and unprotected beams across varying concrete strength grades.

Figs. 21(a-c) and 22(a-c) depict the temperature profiles at T_1 , T_2 and T_3 for M20 and M50 concrete beams, respectively. With reference to T_1 , Figs. 21(a) and 22(a) show that the surface temperatures of the unprotected beams (M20-R and M50-R) closely followed the furnace temperature profile. The protected beams incorporating EV or EP plaster (e.g., M20-EVC, M20-EPC, M50-EVC, M50-EPC) exhibited a significantly lower surface temperature. This reduction was even more pronounced in beams with EV or EP both in the concrete mix and in the plaster (e.g., M20-EV+EVC, M20-EP+EPC, M50-EV+EVC, M50-EP+EPC), highlighting the effectiveness of the protective layer in controlling surface temperature.

On the main rebars at the mid-section of the beam (T_2), Figs. 21(b) and 21(b) show that the unprotected beams experienced the highest temperature profiles at T_2 , while the protected beams with EV or EP in both the mix and plaster achieved the lowest. The results

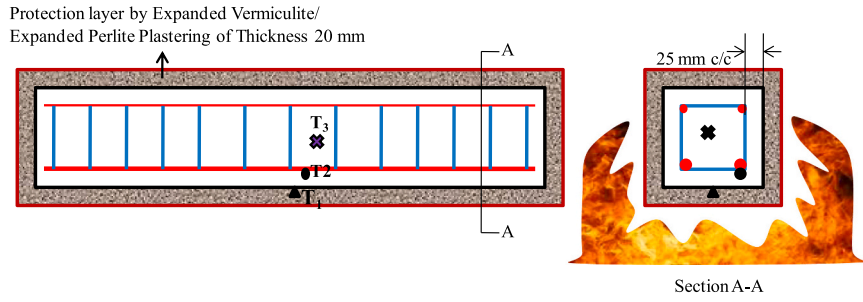


Fig. 20. Locations of the thermocouples in the beam members.

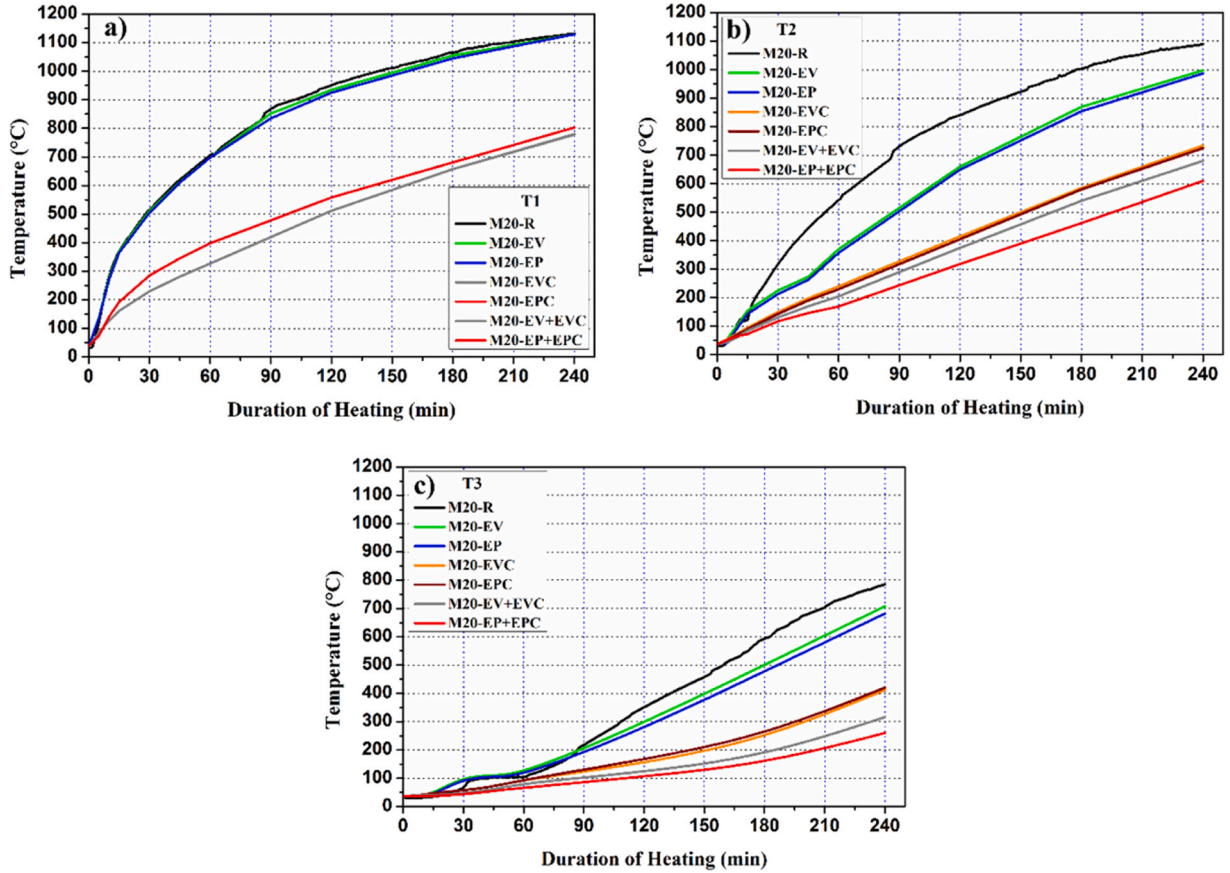


Fig. 21. Development of elevated temperature with time at (a) T₁, (b) T₂ and (c) T₃ for beams made from M20 concrete.

demonstrate that the combination of EV/EP as a lightweight aggregate and as a plaster layer effectively insulated the steel reinforcement, reducing heat transfer significantly. At T₃, the inner core temperature followed a similar trend, with the unprotected beams showing the highest values and the protected beams with EV or EP in both the mix and plaster showing the lowest. Overall, temperatures at all locations (T₁, T₂ and T₃) were higher in the M20 beams compared to the M50 beams. This is attributed to the higher water-cement ratio and lower cement content in the M20 concrete, which increase porosity as hydrated water evaporates at elevated temperatures, facilitating greater heat transfer. Fig. 23 (a) and (b) compare the temperature distributions for the M20 and M50 beams across all measured locations. Beams with external plaster layers exhibited the lowest temperatures at all points, with EP-plastered beams achieving the most significant reductions. This directly correlates with the improved load capacity and performance of these beams under fire exposure, as discussed earlier.

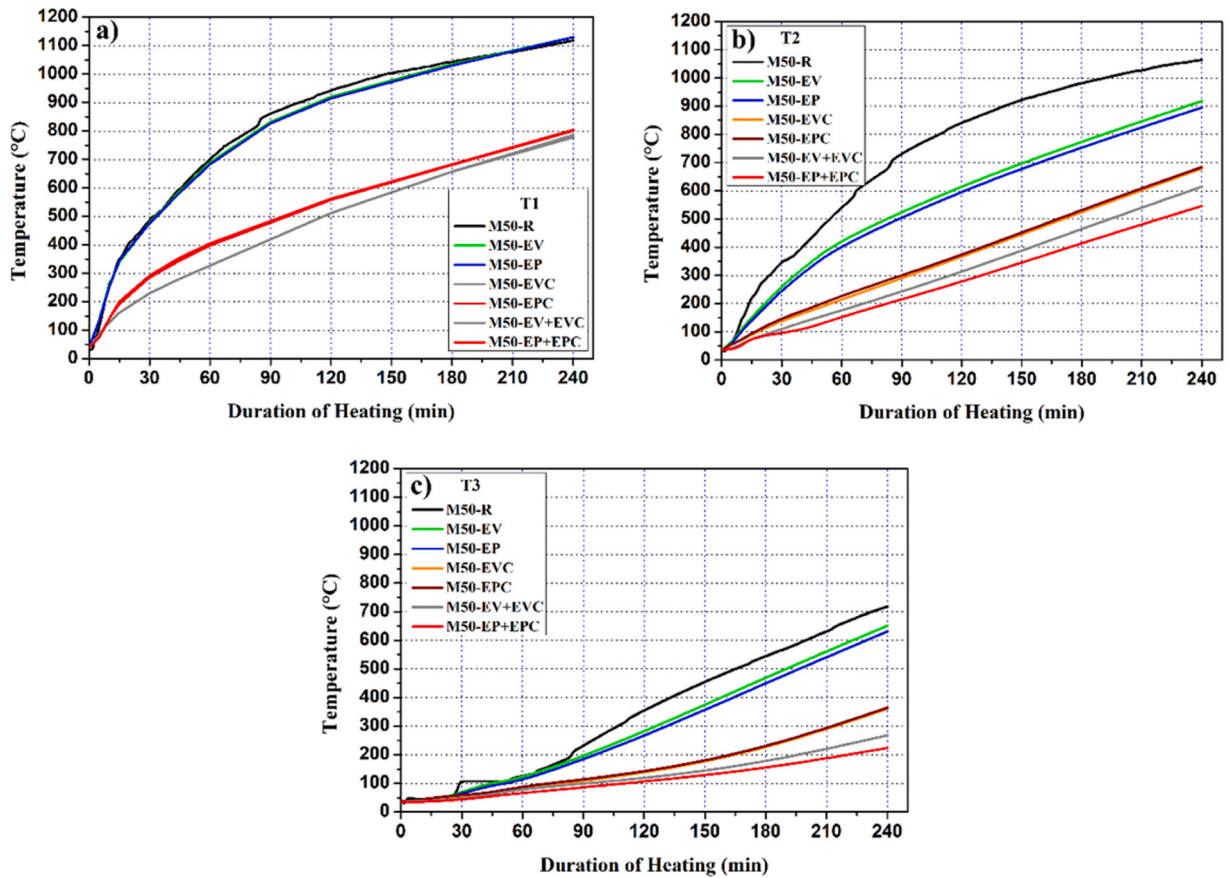


Fig. 22. Development of elevated temperature with time at (a) T_1 , (b) T_2 and (c) T_3 for beams made from M50 concrete.

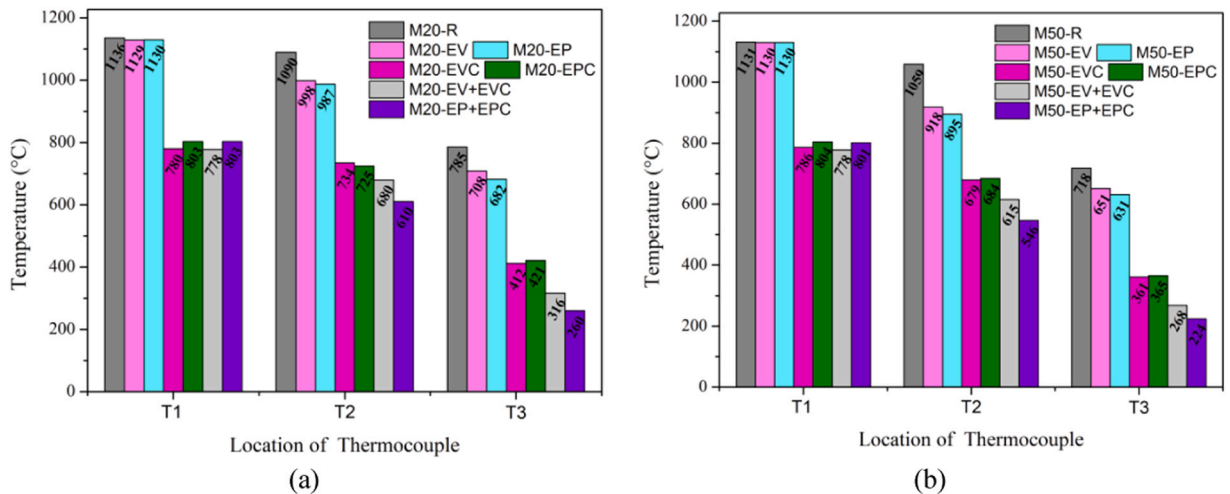


Fig. 23. Variation in maximum temperature reached at different locations for various concrete beams made from (a) M20 concrete and (b) M50 concrete.

4.5. Influence of temperature exposure on the yield strength of reinforcement

The residual effect of elevated temperature on the yield strength of steel reinforcement was evaluated by extracting the steel bars from the tension side of reinforced concrete beam specimens after heating and cooling as illustrated in Fig. 24, and conducting tensile



Fig. 24. Removal of reinforcing bars from test beams and the rebars employed for tensile testing.

tests. The results are shown in Fig. 25 (a) and (b), which illustrate the reduction in yield strength as a ratio of the original value (i.e. reduction factor) for M20 and M50 grade concrete, respectively. A significant difference in residual yield strength was observed between bars from beams containing EV/EP and those from unprotected beams (M20-R and M50-R). The findings were also confirmed by Kodur [27]. Notably, the inclusion of EV or EP in the concrete mix alone was highly effective in minimizing the loss of yield strength, even in the absence of an external plaster layer. This underscores the role of these materials in limiting heat transfer within concrete and protecting the reinforcement from high temperatures. As expected, M20 beams exhibited greater losses in residual yield strength compared to M50 beams, consistent with earlier findings in this study [40,44]. This difference can be attributed to the higher water-cement ratio of M20 concrete, which likely led to increased water evaporation and pore formation during heating, thereby facilitating higher temperatures within the specimen. These results highlight the effectiveness of EV and EP in enhancing the thermal resilience of reinforced concrete systems, particularly in protecting the integrity of steel reinforcement under fire exposure.

4.6. Failure modes and crack patterns

The failure modes and crack patterns provide valuable insights into the residual response of the tested beams, complementing the earlier findings presented. Table 9 summarizes these observations for all of the tested configurations. For unheated M20-R and M50-R beams, vertical cracks initiated at the bottom of the beam within the pure bending region. After 60 min of heating, the protected beams (i.e., M20-EVC, M20-EPC, M20-EV+EVC, and M20-EP+EPC) exhibited inclined cracks, followed by diagonal cracks. In contrast, the unprotected beams (M20-R, M20-EV, and M20-EP) developed diagonal cracks originating from the support regions, ultimately failing in shear due to weakened bond integrity during loading.

For the M50 beams heated for 60 min, vertical cracks initially appeared at mid-span, followed by inclined cracks prior to failure. Prolonging heating to 120 min caused cracks to develop at the support regions of both protected and unprotected M20 beams. The compromised bond between steel and concrete in M20 beams became evident after just 60 min of heating, as shown in Fig. 26. This image highlights concrete separation from steel reinforcement during loading of an M20-EV beam heated for 60 min. Thermal cracks

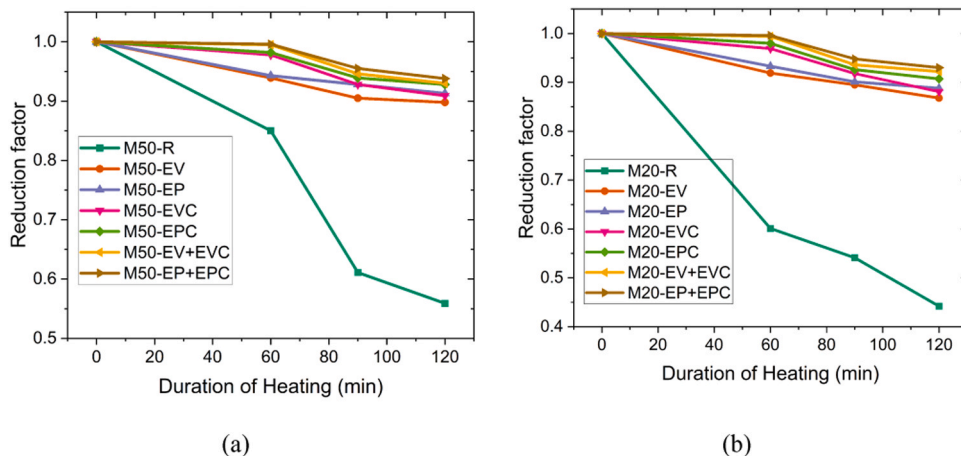
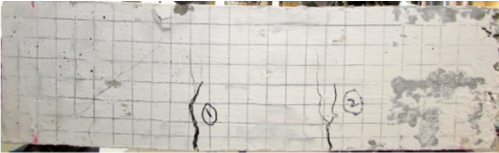
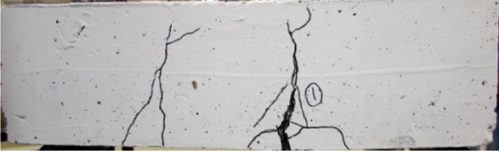
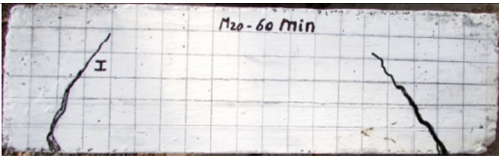
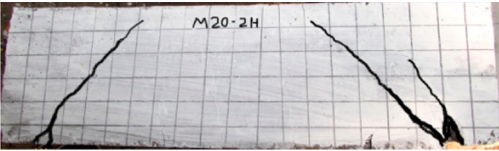
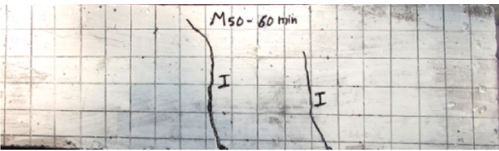
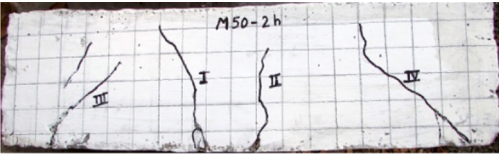

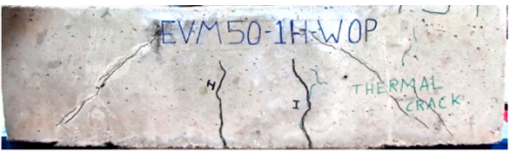
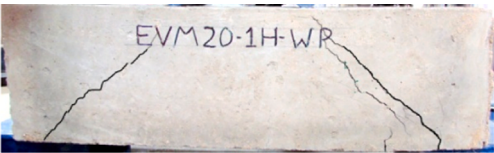


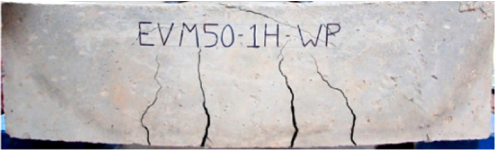
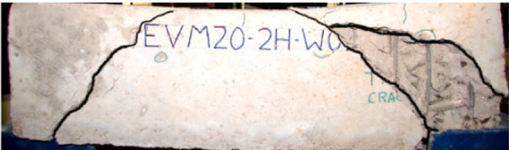


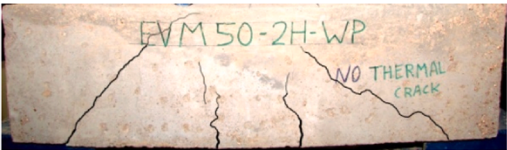

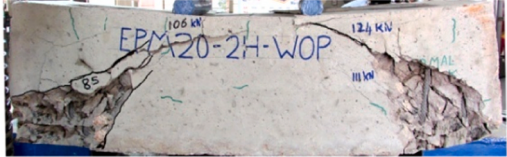
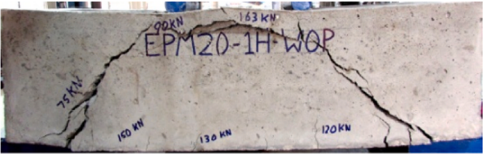

Fig. 25. Reduction factor for yield strength of reinforcement bars following exposure to elevated temperature within concrete beams made from (a) M20 concrete and (b) M50 concrete.

Table 9
Failure Mode and Crack Pattern.

Mix Type	Failure Mode and Crack Pattern	Remarks
M20-R – 0 min		Thermal cracks are observed/ flexural cracks were noted at the mid-span portion during loading/ Flexural failure
M50-R – 0 min		Thermal cracks are observed/ flexural cracks were noted at the mid-span portion during loading/ Flexural failure
M20-R – 60 min		Thermal cracks are observed/ diagonal cracks were noted at the support portion/ shear failure
M20-R – 120 min		Thermal cracks are observed/ diagonal cracks were noted at the support portion/ shear and bond failure
M50-R – 60 min		Thermal cracks are observed/ flexural cracks were noted at the mid-span portion during loading/ Flexural failure
M50-R – 120 min		Flexural yielding of steel followed by diagonal cracks
M20-EV – 60 min		Thermal cracks are observed/ diagonal cracks were noted at the support portion/ shear and bond failure
M50-EV – 60 min		Thermal cracks are observed/ flexural cracks were noted at the mid-span portion followed by inclined cracks during loading/ Flexural and shear failure
M20-EV+EVC – 60 min		No thermal cracks are observed/ diagonal cracks were noted at the support portion/ shear failure

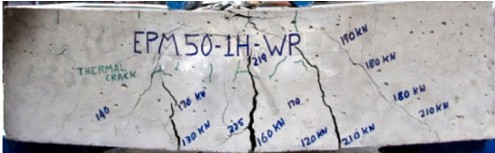
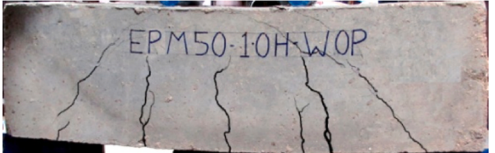
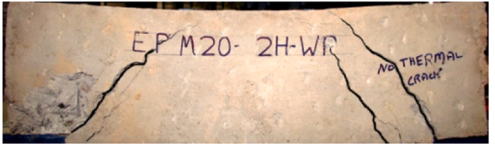

(continued on next page)

Table 9 (continued)

M50-EV+EVC – 60 min		No thermal cracks are observed/ flexural cracks were noted at the mid-span portion during loading/ Flexural failure
M20-EV – 120 min		Thermal cracks are observed/ diagonal cracks were noted at the support portion/ shear and bond failure
M50-EV – 120 min		Thermal cracks are observed/ flexural cracks were noted at the mid-span portion followed by inclined cracks during loading/ Flexural and shear failure
M20-EV+EVC – 120 min		No thermal cracks are observed/ diagonal cracks were noted at the support portion/ shear failure
M50-EV+EPC – 120 min		No thermal cracks are observed/ flexural cracks were noted at the mid-span portion followed by inclined cracks during loading/ Flexural and shear failure
M20-EP+EPC – 60 min		No thermal cracks are observed/ flexural cracks were noted at the mid-span portion during loading/ Flexural failure
M20-EP – 120 min		No thermal cracks are observed/ diagonal cracks were noted at the support portion/ shear and bond failure
M20-EP – 60 min		Thermal cracks are observed/ diagonal cracks were noted at the support portion/ shear and bond failure
M50-EP+EPC – 120 min		No thermal cracks are observed/ flexural cracks were noted at the mid-span portion followed by inclined cracks during loading/ Flexural failure

(continued on next page)

Table 9 (continued)

M50-EP+EPC – 60 min		No thermal cracks are observed/ flexural cracks were noted at the mid-span portion followed by inclined cracks during loading/ Flexural failure
M50-EP – 60 min		Thermal cracks are observed/ flexural cracks were noted at the mid-span portion followed by inclined cracks during loading/ Flexural failure
M20-EP+EPC – 120 min		No thermal cracks are observed/ diagonal cracks were noted at the support portion / shear and bond failure
M50-EP – 120 min		No thermal cracks are observed/ flexural cracks were noted at the mid-span portion followed by inclined cracks during loading/ Flexural and shear failure

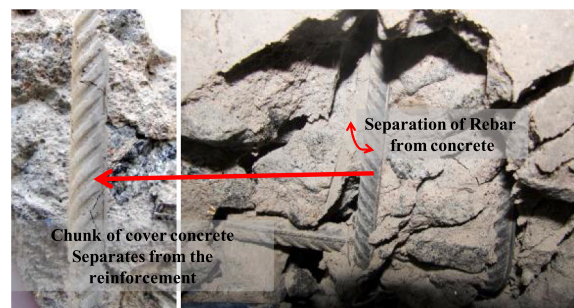


Fig. 26. Failure of bond between concrete and steel from a member exposed to heating for 60 mins followed by cooling.

were observed on the surfaces of unprotected beams during heating, while no such cracks were noted in protected specimens coated with EVC or EPC. This highlights the efficacy of EV and EP plasters in shielding beams from temperature-induced cracking. Further analysis of the EVC and EPC plaster layers, as shown in Fig. 27 (determined using SEM images after 120 min of heating), revealed minor surface deterioration but no significant structural changes. The microstructure of the plasters displayed distributed micro-pores, which dissipate thermal energy effectively, functioning as sacrificial layers to mitigate heat exposure and preserve structural integrity.

4.7. Overall remarks and summary on the behaviour of different RC beams following exposure to elevated temperatures

The results and discussion presented in the previous sub-sections of Section 5 indicate that the inclusion of EV or EP both in the concrete mix, and as a lightweight plaster, has a significant influence on the retention of load capacity and structural integrity following exposure to up to 180 min of standard fire. This means that these materials have the potential to significantly improve the fire performance of RC members, which may be critical for some applications. To complete this analysis, the current section compares the different residual capacity and strength properties, as presented previously. Table 10 presents the variation in residual moment resistance, steel yield strength, and temperatures at T_2 (25 mm from the exposed surface, at the level of the steel reinforcement). It is clear that as the duration of heating increased, both the moment resistance and the yield strength of the reinforcement decreased in all cases. For the unprotected M20-R beam, after 120 min of heating, the steel temperature rose to 841°C , resulting in a 55.96 % reduction in yield strength and a 68.89 % reduction in moment resistance compared to the original unheated specimen. In contrast, the protected M20-EP+EPC beam exhibited significantly better performance under identical conditions: the steel temperature reached only 318°C , leading to a reduction of just 7.02 % in yield strength and 26.79 % in moment resistance. A similar trend was observed for M50 beams,

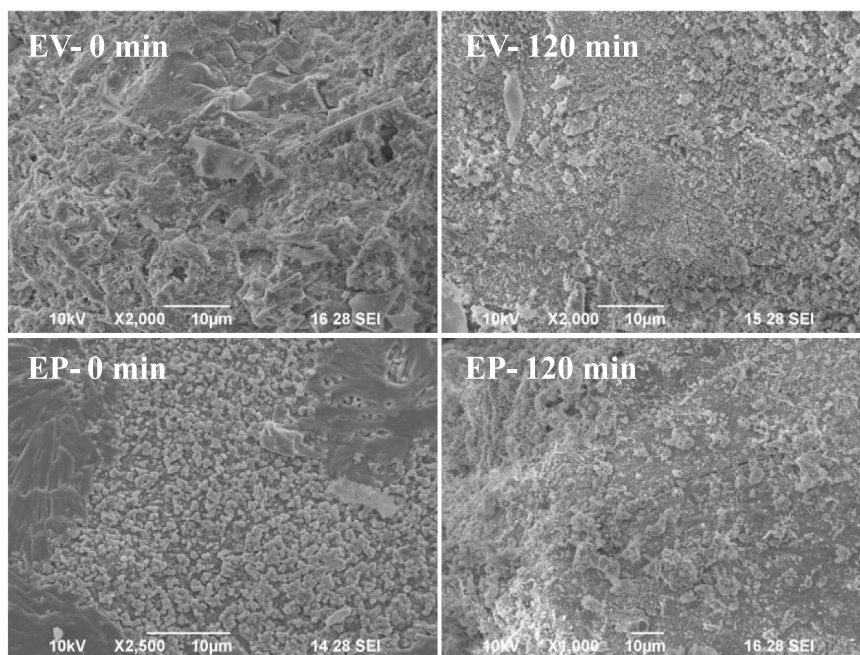


Fig. 27. SEM images of the EP and EV mortar following 0 mins and 120 mins of standard fire exposure.

Table 10

Data of structural performance following exposure to elevated temperatures for beams made from M20 and M50 concrete.

	Duration of heating (min)	Temperature (°C)	Moment of resistance (kNm)	Yield strength (MPa)
M20-R	0	27	20.9	500.0
	60	543	9.2	300.5
	90	731	7.5	270.5
	120	841	6.5	220.2
M20-EP+EPC	0	27	20.9	500.0
	60	169	18.2	497.5
	90	243	17.2	473.9
	120	318	15.3	464.9
M50-R	0	27	24.1	500.0
	60	498	15.8	423.9
	90	731	12.7	305.4
	120	829	9.8	279.3
M50-EP+EPC	0	27	24.1	500.0
	60	155	24.9	497.9
	90	207	23.9	477.2
	120	275	22.8	468.8

which experienced lower reductions in strength and moment resistance than their M20 counterparts. These results underscore the protective effect of external plaster layers and the use of EV/EP in the concrete mix, particularly in limiting heat transfer and preserving the structural integrity of fire-exposed RC beams.

5. Conclusions

This paper presents the details and analysis of a programme of experiments conducted to investigate the post-fire performance of RC beams with either expanded vermiculite (EV) or expanded perlite (EP) included in the design. These materials were incorporated either within the concrete mix, or as a plaster applied to the outer surface, or both of these together, in order to study their influence in preventing or delaying the detrimental effects of fire from affecting the residual structural properties of reinforced concrete beams following exposure to a standard fire. While a common plaster thickness was adopted in the study to enable consistent comparison, it is recognised that in practice, required thicknesses may vary depending on substrate type, thermal insulation demands, and target fire resistance ratings.

The results demonstrated that the fire endurance of RC beams is significantly influenced by the concrete strength grade, water-to-

cement ratio, heating duration, and the type and quantity of lightweight aggregate used. Lower-strength concrete (M20) exhibited poorer residual flexural performance than higher-strength concrete (M50) after fire exposure. However, both grades showed marked improvement in residual strength when EV or EP was incorporated in the mix and applied externally as a protective coating. Beams with combined internal and external EV/EP protection retained between 68 % and 92 % of their original ultimate strength after 60 min of heating, while unprotected reference beams retained only 30 % (M20) and 56 % (M50).

Among the different protection strategies examined, the combination of lightweight aggregate substitution and fire-resistant plastering proved most effective. Expanded perlite plaster (EPC) outperformed vermiculite plaster (EVC) in terms of residual strength retention and temperature reduction. Notably, the yield strength loss of M50-EP+EPC beams after 120 min of heating was limited to 6.24 %, compared to 44.14 % for unprotected M50-R beams. Similarly, EV/EP-modified beams maintained their original flexural failure modes post-fire, in contrast to unprotected specimens, which experienced combined shear and bond failures.

Thermal measurements confirmed that protective coatings significantly reduced internal steel temperatures. For example, the M20-EP+EPC beam recorded a 62.2 % lower rebar temperature and an 87.5 % smaller loss in yield strength compared to its unprotected counterpart. The same beam also showed a 61.1 % reduction in moment resistance degradation, highlighting the effectiveness of EP-based systems in limiting fire-induced damage.

These findings carry several practical implications. The use of EV or EP, particularly in conjunction with protective coatings, offers a viable means of enhancing fire resistance in RC members such as walls, claddings, insulation layers, or non-primary structural elements. Although the results are based on small-scale laboratory specimens, the data provide preliminary insights that can inform the selection of mix proportions, expected strength retention, and thermal performance during design.

However, limitations must be acknowledged. The scale of specimens and simplified boundary conditions used in this study do not fully replicate the behaviour of full-scale elements in real structures. Heat transfer, failure modes, and crack development are scale-dependent, and the controlled loading conditions used differ from the more complex and variable loads encountered in practice. Consequently, the findings should be interpreted as indicative rather than definitive when applied to full-scale structural systems.

Further research is recommended to address these limitations. Future studies should investigate full-scale elements under realistic boundary and loading conditions, and examine the long-term durability of EV/EP concrete under environmental exposures such as chemical attack, freeze-thaw cycles, and moisture ingress. Additionally, comprehensive life-cycle assessments—including initial cost, maintenance, and post-fire repair—are needed to evaluate the economic viability of EV/EP systems. To support broader adoption, further work is also needed to develop codified design guidance for incorporating these materials into performance-based fire engineering approaches.

CRediT authorship contribution statement

Thanaraj Daniel: Writing – original draft, Validation, Resources, Methodology, Investigation, Formal analysis, Data curation, Conceptualization. **N Anand:** Writing – original draft, Validation, Supervision, Resources, Investigation, Funding acquisition, Formal analysis, Data curation, Conceptualization. **Sam Varun:** Validation, Formal analysis, Data curation, Conceptualization. **Diana Andrushia:** Visualization, Validation, Supervision, Formal analysis, Conceptualization. **Cashell Katherine Ann:** Writing – review & editing, Visualization, Validation, Investigation, Formal analysis.

Declaration of Competing Interest

The authors declare that they have no known competing financial interests or personal relationships that could have appeared to influence the work reported in this paper. Daniel Paul Thanaraj, Varun Sabu Sam, Anand N*, Diana Andrushia, Katherine A. Cashell

Data availability

Data will be made available on request.

References

- [1] Y.H. Abdel Aziz, Y. Abdel Zaher, M.A. Wahab, M. Khalaf, Predicting temperature rise in Jacketed concrete beams subjected to elevated temperatures, *Constr. Build. Mater.* 227 (2019) 116460, <https://doi.org/10.1016/j.conbuildmat.2019.07.186>.
- [2] S. Abidi, B. Nait-Ali, Y. Joliff, C. Favotto, Impact of perlite, vermiculite and cement on the thermal conductivity of a plaster composite material: Experimental and numerical approaches, *Compos. Part B Eng.* 68 (2015) 392–400, <https://doi.org/10.1016/j.compositesb.2014.07.030>.
- [3] S. Akçaözoglu, K. Akçaözoglu, C.D. Atiş, Thermal conductivity, compressive strength and ultrasonic wave velocity of cementitious composite containing waste PET lightweight aggregate (WPLA), *Compos. Part B Eng.* 45 (1) (2013) 721–726, <https://doi.org/10.1016/j.compositesb.2012.09.012>.
- [4] K.S. Al-Jabri, M. Hisada, S.K. Al-Oraimi, A.H. Al-Saidy, Copper slag as sand replacement for high performance concrete, *Cem. Concr. Compos.* 31 (7) (2009) 483–488, <https://doi.org/10.1016/j.cemconcomp.2009.04.007>.
- [5] K. Al-Jabri, H. Shoukry, Use of nano-structured waste materials for improving mechanical, physical and structural properties of cement mortar, *Constr. Build. Mater.* 73 (2014) 636–644, <https://doi.org/10.1016/j.conbuildmat.2014.10.004>.
- [6] American Concrete Institute. (2007). Fire resistance design of concrete structures (ACI 216R-07). American Concrete Institute.
- [7] D.A. Andrushia, N. Anand, P.G. Arulraj, A novel approach for thermal crack detection and quantification in structural concrete using ripplet transform, *Struct. Control Health Monit.* 27 (11) (2020), <https://doi.org/10.1002/stc.2621>.
- [8] P.C.D. Assis Neto, L.P.B. Sales, P.K.S. Oliveira, I.C.D. Silva, I.M.D.S. Barros, A.F.D. Nóbrega, A.M.P. Carneiro, Expanded vermiculite: a short review about its production, characteristics, and effects on the properties of lightweight mortars, *Buildings* 13 (3) (2023) 823, <https://doi.org/10.3390/buildings13030823>.
- [9] Z. Azimi, M. Mousavi, H.A. Bengar, A.A. Javadi, Post-fire properties of lightweight 3D printed concrete containing expanded perlite, *Mag. Concr. Res.* 76 (10) (2023) 523–534, <https://doi.org/10.1680/jmacr.23.00159>.

- [10] A. Benli, M. Karataş, Y. Bakir, An experimental study of different curing regimes on the mechanical properties and sorptivity of self-compacting mortars with fly ash and silica fume, *Constr. Build. Mater.* 144 (2017) 552–562, <https://doi.org/10.1016/j.conbuildmat.2017.03.228>.
- [11] A.R.D. Carvalho, A.H.G. Casali, G.D. Silva, R.P. Pita, M.C.R. Farage, T.M.D. Oliveira, Analysis of the thermomechanical behavior of different concretes with vermiculite and submitted to elevated temperatures, *REMInt. Eng. J.* 77 (3) (2024) e230079, <https://doi.org/10.1590/0370-44672023770079>.
- [12] Dias, Mechanical properties of hardened cement paste exposed to temperatures up to 700C (1292 F), *Acids Mater. J.* 87 (2) (1990), <https://doi.org/10.14359/1981>.
- [13] G. Durmuş, H.C. Topuz, Thermal characterization of foam concrete panels containing expanded perlite-polystyrene, foam and aerogel layer, *Gazi Üniversitesi Fen. Bilim. Derg. Part C Tasar. İM. ve Teknol.* 10 (1) (2022) 39–49, <https://doi.org/10.29109/gujsc.1015369>.
- [14] S.M.A. El-Gamal, F.S. Hashem, M.S. Amin, Thermal resistance of hardened cement pastes containing vermiculite and expanded vermiculite, *J. Therm. Anal. Calorim.* 109 (1) (2012) 217–226, <https://doi.org/10.1007/s10973-011-1680-9>.
- [15] H.Z. El-Karmoty, Thermal protection of reinforced concrete columns strengthened by GFRP laminates (experimental and theoretical study), *HBRC J* 8 (2) (2012) 115–122, <https://doi.org/10.1016/j.hbrj.2012.09.007>.
- [16] Eurocode 2, *Design of concrete structures – Part 1-2: General rules – Structural fire design (EN 1992-1-2)*, European Committee for Standardization, 2004.
- [17] J. Formosa-Mitjans, L. Haurie, J.M. Chimenos-Ribera, A.M. Lacasta, J.R. Rosell, Comparative study of magnesium by-prebaructs and vermiculite formulations to obtain fire resistant mortars, *Mater. Sci. Forum* 587–588 (2008) 898–902, <https://doi.org/10.4028/www.scientific.net/MSF.587-588.898>.
- [18] A.S. Gandage, V.R.V. Rao, M.V.N. Sivakumar, A. Vasan, M. Venu, A.B. Yaswanth, Effect of perlite on thermal conductivity of self compacting concrete, *Procedia Soc. Behav. Sci.* 104 (2013) 188–197, <https://doi.org/10.1016/j.sbspro.2013.11.111>.
- [19] O. Gencel, F. Koksall, M. Sahin, M.Y. Durgun, H.E.H. Lobland, W. Brostow, Modeling of thermal conductivity of concrete with vermiculite by using artificial neural networks approaches, *Exp. Heat. Transf.* 26 (4) (2013) 360–383, <https://doi.org/10.1080/08916152.2012.669810>.
- [20] O.A. Hodhod, A.M. Rashad, M.M. Abdel-Razek, A.M. Ragab, Coating protection of loaded RC columns to resist elevated temperature, *Fire Saf. J.* 44 (2) (2009) 241–249, <https://doi.org/10.1016/j.firesaf.2008.06.010>.
- [21] K.M.A. Hossain, S. Ahmed, M. Lachemi, Lightweight concrete incorporating pumice based blended cement and aggregate: mechanical and durability characteristics, *Constr. Build. Mater.* 25 (3) (2011) 1186–1195, <https://doi.org/10.1016/j.conbuildmat.2010.09.036>.
- [22] ISO 834-1. (1999). Fire-resistance tests-Elements of building construction-Part 1: General requirements. ISO Standard, STD-615580.
- [23] B. Kanagaraj, N. Anand, R.S. Raj, E. Lubloy, Performance evaluation on engineering properties of sodium silicate binder as a precursor material for the development of cement-free concrete, *Dev. Built Environ.* 12 (2022) 100092, <https://doi.org/10.1016/j.dibe.2022.100092>.
- [24] M.B. Karakoç, Effect of cooling regimes on compressive strength of concrete with lightweight aggregate exposed to high temperature, *Constr. Build. Mater.* 41 (2013) 21–25, <https://doi.org/10.1016/j.conbuildmat.2012.11.104>.
- [25] M. Karatas, A. Benli, H.A. Toprak, Effect of incorporation of raw vermiculite as partial sand replacement on the properties of self-compacting mortars at elevated temperature, *Constr. Build. Mater.* 221 (2019) 163–176, <https://doi.org/10.1016/j.conbuildmat.2019.06.077>.
- [26] G.A. Khoury, Compressive strength of concrete at high temperatures: a reassessment, *Mag. Concr. Res.* 44 (161) (1992) 291–309, <https://doi.org/10.1680/mac.1992.44.161.291>.
- [27] V. Kodur, *Properties of concrete at elevated temperatures*, *Int. Sch. Res. Not.* 2014 (1) (2014) 468510.
- [28] V. Kodur, M.Z. Naser, *Structural fire engineering*, McGraw-Hill Education, 2020.
- [29] F. Koksall, O. Gencel, M. Kaya, Combined effect of silica fume and expanded vermiculite on properties of lightweight mortars at ambient and elevated temperatures, *Constr. Build. Mater.* 88 (2015) 175–187, <https://doi.org/10.1016/j.conbuildmat.2015.04.021>.
- [30] F. Koksall, T. Nazlı, A. Benli, O. Gencel, G. Kaplan, The effects of cement type and expanded vermiculite powder on the thermo-mechanical characteristics and durability of lightweight mortars at high temperature and RSM modelling, *Case Stud. Constr. Mater.* 15 (2021) e00709, <https://doi.org/10.1016/j.cscm.2021.e00709>.
- [31] K. Krzemień, I. Hager, Assessment of concrete susceptibility to fire spalling: a report on the state-of-the-art in testing procedures, *Procedia Eng.* 108 (2015) 285–292, <https://doi.org/10.1016/j.proeng.2015.06.149>.
- [32] Z. Li, X. Zhou, B. Shen, Fiber-cement extrudates with perlite subjected to high temperatures, *J. Mater. Civ. Eng.* 16 (3) (2004) 221–229, [https://doi.org/10.1061/\(ASCE\)0899-1561\(2004\)16:3\(221\)](https://doi.org/10.1061/(ASCE)0899-1561(2004)16:3(221)).
- [33] L. Lim, A. Buchanan, Fire behavior of slender precast concrete walls, *Fire Saf. Sci.* 7 (2003) 1135–1146, <https://doi.org/10.3801/IAFSS.FSS.7-1135>.
- [34] C. Liu, Z. Qiu, S. Zhang, L. Yan, J. Miao, C. Zheng, Experimental study on dynamic bond behavior between reinforcement and concrete under fire, *J. Mater. Civ. Eng.* 36 (6) (2024) 04024140, <https://doi.org/10.1061/JMCEE7.MTENG.1765>.
- [35] J. Liu, Y. Zhuhe, X. Ma, M. Liu, Y. Liu, X. Wu, H. Xu, Physical and mechanical properties of expanded vermiculite (EV) embedded foam concrete subjected to elevated temperatures, *Case Stud. Constr. Mater.* 16 (2022) e01038, <https://doi.org/10.1016/j.cscm.2022.e01038>.
- [36] C. Martias, Y. Joliff, C. Favotto, Effects of the addition of glass fibers, mica and vermiculite on the mechanical properties of a gypsum-based composite at room temperature and during a fire test, *Compos. Part B Eng.* 62 (2014) 37–53, <https://doi.org/10.1016/j.compositesb.2014.02.019>.
- [37] K.H. Mo, H.J. Lee, M.Y.J. Liu, T.-C. Ling, Incorporation of expanded vermiculite lightweight aggregate in cement mortar, *Constr. Build. Mater.* 179 (2018) 302–306, <https://doi.org/10.1016/j.conbuildmat.2018.05.219>.
- [38] M. Mohammad, E. Masad, T. Seers, S.G. Al-Ghamdi, Properties and microstructure distribution of high-performance thermal insulation concrete, *Materials* 13 (9) (2020) 2091, <https://doi.org/10.3390/ma13092091>.
- [39] NBC (National building code of India), Part 4: Fire and Life Safety, Bureau of Indian Standards, 2016, Newdelhi.
- [40] L.T. Phan, N.J. Carino, Effects of test conditions and mixture proportions on behavior of high-strength concrete exposed to high temperatures, *Acids Mater. J.* 99 (1) (2002) 54–66.
- [41] J. Pizoń, P. Konečný, M. Mynarz, V. Bílek, Properties of fine graded perlite-based lightweight cement mortars subjected to elevated temperatures, *Buildings* 13 (12) (2023) 2969, <https://doi.org/10.3390/buildings13122969>.
- [42] J. Purkiss, *Fire Safety Engineering Design of Structures*, Second ed., CRC Press, 2007, 10.1201/b12845.
- [43] A.M. Rashad, Vermiculite as a construction material – A short guide for Civil Engineer, *Constr. Build. Mater.* 125 (2016) 53–62, <https://doi.org/10.1016/j.conbuildmat.2016.08.019>.
- [44] N.K. Raut, V.K.R. Kodur, Response of high-strength concrete columns under design fire exposure, *J. Struct. Eng.* 137 (1) (2011) 69–79.
- [45] V. Sabu Sam, M.S. Adarsh, G.R. Lyngdoh, G.W.K. Marak, N. Anand, K. Al-Jabri, D. Andrushia, Influence of elevated temperature on buckling capacity of mild steel-based cold-formed steel column sections– experimental investigation and finite element modelling, *J. Struct. Fire Eng. AheadPrint. (AheadPrint)* (2023), <https://doi.org/10.1108/JSFE-08-2023-0033>.
- [46] V. Sabu Sam, A. N, K. Marak, G.W. Lyngdoh, G.R. Alengaram, J. Diana Andrushia, Investigation on residual mechanical properties of galvanized iron cold-formed steel sections exposed to elevated temperatures, *Electron. J. Struct. Eng.* 24 (1) (2024) 53–59, <https://doi.org/10.56748/ejse.24439>.
- [47] A.E. Salama, G.M. Ghanem, S.F. Abd-Elnaby, A.A. El-Hefnawy, M. Abd-Elghaffar, Behavior of thermally protected RC beams strengthened with CFRP under dual effect of elevated temperature and loading, *HBRC J.* 8 (1) (2012) 26–35, <https://doi.org/10.1016/j.hbrj.2012.08.005>.
- [48] A. Schackow, C. Efting, M.V. Folgueras, S. Güths, G.A. Mendes, Mechanical and thermal properties of lightweight concretes with vermiculite and EPS using air-entraining agent, *Constr. Build. Mater.* 57 (2014) 190–197, <https://doi.org/10.1016/j.conbuildmat.2014.02.009>.
- [49] S. Sharook, D. Sathyan, M.K. Madhavan, Thermo-mechanical and durability properties of expanded perlite aggregate foamed concrete, *Proc. Inst. Civ. Eng. Constr. Mater.* 176 (4) (2020) 141–149, <https://doi.org/10.1680/jcoma.20.00041>.
- [50] X. Shi, T.-H. Tan, K.-H. Tan, Z. Guo, Influence of concrete cover on fire resistance of reinforced concrete flexural members, *J. Struct. Eng.* (2004), [https://doi.org/10.1061/\(asce\)0733-9445\(2004\)130:8\(1225\)](https://doi.org/10.1061/(asce)0733-9445(2004)130:8(1225)).
- [51] T.J. Shields, G.W.H. Silcock, M.F. Flood, Performance of a single glazing assembly exposed to enclosure corner fires of increasing severity, *Fire Mater.* 25 (4) (2001) 123–152, <https://doi.org/10.1002/fam.764>.

- [52] M. Sutcu, Influence of expanded vermiculite on physical properties and thermal conductivity of clay bricks, *Ceram. Int.* 41 (2, Part B) (2015) 2819–2827, <https://doi.org/10.1016/j.ceramint.2014.10.102>.
- [53] D.P. Thanaraj, N. Anand, G. Prince Arulraj, E. Zalok, Post-fire damage assessment and capacity based modeling of concrete exposed to elevated temperature, *Int. J. Damage Mech.* 29 (5) (2020) 748–779, <https://doi.org/10.1177/1056789519881484>.
- [54] D.P. Thanaraj, A. N, P. Arulraj, Experimental investigation of mechanical properties and physical characteristics of concrete under standard fire exposure, *J. Eng. Des. Technol.* 17 (5) (2019) 878–903, <https://doi.org/10.1108/JEDT-09-2018-0159>.
- [55] D.P. Thanaraj, A. N, P. Arulraj, K. Al-Jabri, Investigation on structural and thermal performance of reinforced concrete beams exposed to standard fire, *J. Build. Eng.* 32 (2020) 101764, <https://doi.org/10.1016/j.job.2020.101764>.
- [56] İ. Türkmen, A. Kantarcı, Effects of expanded perlite aggregate and different curing conditions on the physical and mechanical properties of self-compacting concrete, *Build. Environ.* 42 (6) (2007) 2378–2383, <https://doi.org/10.1016/j.buildenv.2006.06.002>.
- [57] I. Uluşu, A. Kurnuc Seyhan, Effect of Expanded Perlite Aggregate Plaster on the Behavior of High-Temperature Reinforced Concrete Structures, *Buildings* 13 (2) (2023) 384, <https://doi.org/10.3390/buildings13020384>.
- [58] A. Varghese, A. N, P. Arulraj G, U. Johnson Alengaram, Influence of fibers on bond strength of concrete exposed to elevated temperature, *J. Adhes. Sci. Technol.* 33 (14) (2019) 1521–1543, <https://doi.org/10.1080/01694243.2019.1602889>.
- [59] Z. Wu, S. Huen Lo, K. Hai Tan, K. Leung Su, High strength concrete tests under elevated temperature, *Athens J. Technology Eng.* 6 (3) (2019) 141–162, <https://doi.org/10.30958/ajte.6-3-1>.